REPORT DOCUMENTATION PAGE

AFRL-SR-AR-TR-03-

0031

1. REPORT DATE *(DD-MM-YYYY)*	2. REPORT TYPE	3. DATES COVERED *(From - To)*
27-01-2003	Final	Mar 2002 - Jan 2003

4. TITLE AND SUBTITLE

STRUCTURE AND MODELING OF OPTICAL WAVEFRONTS IN HIGH-REYNOLDS-NUMBER TURBULENT AERO-OPTIC FLOWS

5a. CONTRACT NUMBER

5b. GRANT NUMBER
F49620-02-1-0142

5c. PROGRAM ELEMENT NUMBER

6. AUTHOR(S)

Catrakis, Haris, J.

5d. PROJECT NUMBER

5e. TASK NUMBER

5f. WORK UNIT NUMBER

7. PERFORMING ORGANIZATION NAME(S) AND ADDRESS(ES)

Prof. Haris J. Catrakis, Principal Investigator
Aeronautics and Fluid Dynamics Laboratories
University of California, Irvine
4200 Engineering Gateway
Irvine, CA 92697-3975

8. PERFORMING ORGANIZATION REPORT NUMBER

9. SPONSORING / MONITORING AGENCY NAME(S) AND ADDRESS(ES)

Dr. Thomas J. Beutner, Program Manager
Turbulence and Rotating Flows
Air Force Office of Scientific Research
4015 Wilson Boulevard, Room 713
Arlington, VA 22203-1954

10. SPONSOR/MONITOR'S ACRONYM(S)

11. SPONSOR/MONITOR'S REPORT NUMBER(S)

12. DISTRIBUTION / AVAILABILITY STATEMENT

Unlimited distribution

20030305 093

13. SUPPLEMENTARY NOTES

14. ABSTRACT

Two new methods have been developed and demonstrated which are particularly useful for modeling the large-scale and small-scale structure of aerooptical distortions, as well as the refractive fluid interfaces or density interfaces responsible for these distortions, at high compressibility and large Reynolds numbers. The first method, termed the interfacial-thickness approach, enables the examination of optical-wavefront propagation in terms of the physical thickness of the refractive interfaces. Demonstration of this method on experimental data in high-compressibility large-Reynolds-number shear layers has revealed that the high-gradient regions are spatially isolated. This observation has been utilized to propose and demonstrate a new modeling approach where the high-gradient interfaces are the dominant elements necessary to reproduce the large-scale optical distortions at high compressibility. The second method enables the characterization of the physical anisotropic structure of aerooptical wavefronts as a function of scale. This is useful to extrapolate the small-scale structure of aerooptical distortions at high compressibility to larger Reynolds numbers. These two new techniques enable the modeling of large-scale and small-scale aerooptical behavior at high-compressibility flow conditions relevant to high-speed flight, and are important for Air Force applications involving laser beam propagation in high-speed flight such as for tactical fighter aircraft.

15. SUBJECT TERMS

Large-scale and small-scale aerooptical distortions, high compressibility, large Reynolds numbers, tactical fighter aircraft, laser beam propagation, optical imaging, refractive turbulent fluid interfaces, aerooptical wavefronts, interfacial-thickness approach.

16. SECURITY CLASSIFICATION OF:			17. LIMITATION OF ABSTRACT	18. NUMBER OF PAGES	19a. NAME OF RESPONSIBLE PERSON
U			UU	43	Prof. Haris J. Catrakis
a. REPORT	b. ABSTRACT	c. THIS PAGE			19b. TELEPHONE NUMBER *(include area code)*
U	U	U			(949) 378-7781

Grant Report to the Air Force Office of Scientific Research

AFOSR Grant F49620-02-1-0142

Structure And Modeling Of Optical Wavefronts In High-Reynolds-Number Turbulent Aero-Optic Flows

Haris J. Catrakis

Aeronautics and Fluid Dynamics Laboratories
University of California, Irvine

Grant period: March 1, 2002 to October 31, 2002

Funds awarded in this Grant period: $20,000

AFOSR Program Manager:

Dr. Thomas J. Beutner
Program Manager
Turbulence and Rotating Flows
Aerospace and Materials Sciences Directorate
Air Force Office of Scientific Research

4015 Wilson Boulevard, Room 713
Arlington, VA 22203-1954
Phone: (703) 696-6961
Fax: (703) 696-8451
E-mail: tom.beutner@afosr.af.mil

Principal Investigator:

Dr. Haris J. Catrakis
Assistant Professor
Turbulence and the Dynamics of Fluids
Aeronautics and Fluid Dynamics Laboratories
University of California, Irvine

4200 Engineering Gateway
Irvine, CA 92697-3975
Phone: (949) 378-7781
Fax: (949) 824-8585
E-mail: catrakis@uci.edu

AFRL Point of Contact:

Mr. Rudy Martinez
Strategic Planner
Directed Energy Directorate
Kirtland Air Force Base
Air Force Research Laboratories

3550 Aberdeen Avenue
Albuquerque, NM 87117-5776
Phone: (505) 846-9848
Fax: N/A
E-mail: rudy.martinez@kirtland.af.mil

January 27, 2003

Abstract

Two new methods have been developed and demonstrated which are particularly useful for modeling the large-scale and small-scale structure of aerooptical distortions, as well as the refractive fluid interfaces or density interfaces responsible for these distortions, at high compressibility and large Reynolds numbers. The first method, termed the interfacial-thickness approach, enables the examination of optical-wavefront propagation in terms of the physical thickness of the refractive interfaces and is particularly useful for modeling the large-scale aerooptical distortions at high compressibility. At large Reynolds numbers and high compressibility, the interfacial thickness is highly variable. We have shown that this thickness plays an important role in aerooptics by expressing the optical path length (OPL) directly in terms of the interfacial-thickness variations. Application of the interfacial-thickness approach to experimental data in high-compressibility ($M_c \sim 1$) large-Reynolds-number ($Re \sim 10^6$) shear layers reveals isolated sheet-like regions of high refractive-gradient magnitudes at various transverse locations in the flow, i.e. both in the interior and near the outer boundaries, that form highly-irregular networks. The observation that the high-gradient regions are spatially-isolated interfaces, and the interpretation of the OPL in terms of interfacial-thickness variations, are utilized to propose and demonstrate a new modeling approach where the high-gradient interfaces are the dominant elements necessary to reproduce the large-scale optical distortions at high compressibility. This new modeling methodology provides the means to model the large-scale optical distortions in terms of the high-gradient interfaces, at high compressibility. The second method developed in this grant enables the characterization of the physical structure of aerooptical wavefronts as a function of scale, and is particularly important for modeling the small-scale structure of aerooptical distortions at high compressibility. Because turbulence-degraded optical wavefronts are physically highly anisotropic and exhibit distortions which span a wide range of scales at large Reynolds numbers, a technique is needed which enables a scale-local examination of wavefronts at varying degrees of anisotropy. We have defined an optical-anisotropy parameter as a ratio of scaling factors for the OPL and spatial extent of the wavefronts. This parameter, in combination with box-counting techniques, enables the study of the scale-local and anisotropic structure of wavefronts. Application to high-compressibility large-Reynolds-number data, and variation of the anisotropy parameter, shows the presence of anisotropic self-similarity in the wavefront OPL over a wide range of small scales. This finding is important because it provides a means to extrapolate the small-scale structure of aerooptical distortions at high compressibility to larger Reynolds numbers. In summary, we have developed and demonstrated two new techniques which are particularly useful for describing the large-scale as well as small-scale aerooptical behavior in high-compressibility flows. We have shown that both techniques are valuable for modeling aerooptical distortions at flow conditions relevant to high-speed flight. The two new techniques can also be expected to be valuable for predicting as well as controlling aerooptical interactions at high compressibility. These two techniques are important for Air Force applications involving laser beam propagation in high-speed flight relevant for tactical fighter aircraft.

---

1. Overview of publications, presentations, personnel, and AFRL interactions

Publications:

The major results of the work done in this grant are two new approaches developed and demonstrated by the PI and his students to examine the large-scale and small-scale structure of aerooptical distortions and refractive fluid interfaces at high compressibility and large Reynolds numbers. These two approaches have been submitted as two journal papers currently under consideration for publication in the *AIAA Journal*:

"New Interfacial-Thickness Approach in Aerooptics and Large-Scale Optical Distortions in High-Compressibility Turbulence," Catrakis, H. J. and Aguirre, R. C., *AIAA Journal*, submitted for publication.

"Aerooptical-Wavefront Anisotropy and Small-Scale Structure at Large Reynolds Numbers and High Compressibility," Catrakis, H. J., Aguirre, R. C., and Ruiz-Plancarte, J., *AIAA Journal*, submitted for publication.

Presentations and refereed conference papers:

The new interfacial-thickness approach in aerooptics and the anisotropic-characterization technique for aerooptical wavefronts, as well as their demonstration to experimental data at high compressibility and large Reynolds numbers, have been presented at two AIAA conferences:

"Physical Thickness of Turbulent Fluid Interfaces: Structure, Variability, and Applications to Aerooptics," Aguirre, R. C., Ruiz-Plancarte, J., and Catrakis, H. J., 41st *AIAA Aerospace Sciences Meeting and Exhibit, Reno, NV, AIAA Paper 2003-0642.*

"Internal-Scale Structure of Turbulence-Degraded Optical Wavefronts," Catrakis, H. J. and Aguirre, R. C., 33rd *AIAA Plasmadynamics and Lasers Conference, Maui, HI, AIAA Paper 2002-2269.*

Personnel involved:

In addition to the PI, one primary graduate student is involved in this work, Roberto C. Aguirre, who is conducting his Ph.D. thesis research in aerooptics. Another graduate student, Jesus Ruiz-Plancarte, is also assisting with the aerooptics research as part of his Ph.D. thesis research.

Haris J. Catrakis	Assistant Professor, University of California, Irvine
Roberto C. Aguirre	Graduate Student, University of California, Irvine
Jesus Ruiz-Plancarte	Graduate Student, University of California, Irvine

AFRL interactions:

The PI has initiated contact with Rudy Martinez (AFRL, Kirtland AFB, Albuquerque, NM)) who is a Strategic Planner in the Directed-Energy Directorate. Mr. Martinez is the AFRL Point-of-Contact (POC) for the PI. The AFRL POC is interested in aerooptics for high-speed and high-maneuverability aircraft, such as tactical fighter aircraft, for example the Joint Strike Fighter (JSF) by Lockheed Martin. For these aerooptics applications, the PI's two new aerooptics approaches are particularly useful. The PI has also been interacting with Dr. Michael Jones of Lockheed Martin (Ft. Worth, TX). The two new aerooptics characterization methods developed by the PI are of potential use in computational simulation codes and war-game simulators at AFRL and also Lockheed Martin.

2. Research results

The main research results in this grant are the two new approaches in aerooptics developed and demonstrated by the PI. They are described in detail in the two papers submitted to *AIAA Journal* ([1] Catrakis & Aguirre 2003, and [2] Catrakis, Aguirre, & Ruiz-Plancarte 2003). In the present section, the two techniques are also described.

New interfacial-thickness approach and its demonstration on the examination and modeling of large-scale optical distortions in high-compressibility turbulence:

In order to develop techniques for the prediction and control of aerooptical phenomena in turbulent flows, an improved understanding is needed of the large-scale properties and, for some applications, of the small-scale properties of aerooptical distortions as well as of the turbulent refractive fluid interfaces that generate these distortions (e.g. [3] Jumper & Fitzgerald 2001, and references therein). Practically, the large-scale aerooptical behavior is crucial in all applications involving optical beam propagation or imaging through turbulent shear flows, such as the flows generated by airborne vehicles. The small-scale behavior can also be important for those applications that require high-resolution and/or long-range optical imaging or beam propagation. In addition, it is important to know in practice the behavior of aerooptical interactions at large Reynolds numbers. Furthermore, for high-speed flight, it is also crucial to quantify Mach-number effects on the aerooptical behavior (e.g. [4] Gilbert & Otten 1982, and references therein).

The large-scale organized flow behavior is known to provide the dominant aerooptical contributions in both incompressible turbulent flows (e.g. [5] Truman & Lee 1990; [6] Wissler & Roshko 1992; [7] Dimotakis, Catrakis, & Fourguette 2001) and weakly-compressible turbulent flows (e.g. [3] Jumper & Fitzgerald 2001). At higher flow compressibilities, however, the extent to which the large-scale flow behavior is organized is not well understood (e.g. [8] Smits & Dussauge 1996; [7] Dimotakis, Catrakis, & Fourguette 2001). The large-scale properties of aerooptical distortions at high compressibility, and the manner in which they are related to the fluid-interfacial behavior, are also not well understood.

Since the pioneering aerooptics studies by Liepmann (1952 [9], 1952b [10]), it has been recognized that one of the central goals in aerooptics research is to relate the optical-

wavefront distortions to the fluid-mechanical behavior. The optical-wavefront distortions are usefully quantified by the optical path length (OPL), here denoted as $\Lambda(\mathbf{x},t)$, for many aerooptics applications. The most relevant fluid-mechanical quantity in aerooptics is the refractive-index field,

$$n(\mathbf{x},t) \equiv \frac{c_0}{c(\mathbf{x},t)} \geq 1 \,, \tag{1}$$

where $c(\mathbf{x},t)$ is the local speed of light which is always less than or equal to Einstein's universal speed of light c_0 in vacuum and independent of the frame of reference. In turbulent flows, the refractive-index field $n(\mathbf{x},t)$ can be highly nonuniform particularly at large Reynolds numbers and at high compressibility. The propagation of optical wavefronts through refractive-index fields is governed by the eikonal equation,

$$|\nabla\Lambda| = n \,, \tag{2}$$

where, as stated above, Λ denotes the OPL. The eikonal equation is useful to describe fluid-optical interactions as long as the wavelength of light is smaller than the smallest fluid-mechanical (turbulent) scale (e.g. [9] Liepmann 1952) and as long as the optical-beam energies are low enough to not change the local refractive index. If these conditions are not satisfied, one needs to resort to wave optics using Maxwell's equations or, if the quantization of energy of light plays a direct role, Feynman's quantum-electrodynamics description. We note that while the eikonal equation 2 is derivable from the general variational principle of Fermat, which is a principle of least time of optical propagation in most cases, the governing equations of fluid mechanics and of turbulent flows, i.e. the Navier-Stokes equations, have not yet been related to any general variational principle.

How is the OPL behavior related physically to the structure of the refractive-index field and in particular the refractive fluid interfaces? We have developed a framework that is useful to address this question by emphasizing the role of the physical thickness of the refractive fluid interfaces in determining the variations in the OPL.

Our starting point is the expression used for the definition of the OPL as an integral of the refractive index along each light ray in geometric optics (e.g. [7] Dimotakis, Catrakis, & Fourguette 2001; [3] Jumper & Fitzgerald 2001, and references therein), i.e.,

$$\Lambda(\mathbf{x},t) \equiv \int_{\text{ray}} n(\ell,t)\,\mathrm{d}\ell \,, \tag{3}$$

where again Λ denotes the OPL and ℓ denotes the physical distance along the propagation path of each light ray. The OPL integral in equation 3 corresponds to inverting the eikonal equation 2 for the OPL in terms of the refractive-index field. The aerooptical distortions correspond to the optical-path difference (OPD) given by $\Delta\Lambda(\mathbf{x},t) \equiv \Lambda(\mathbf{x},t) - \Lambda_{\text{ref}}(\mathbf{x},t)$, where $\Lambda_{\text{ref}}(\mathbf{x},t) \equiv \int_{\text{ray}} n_{\text{ref}}(\mathbf{x},t)\,\mathrm{d}\ell$ is the reference OPL that would correspond to the undistorted wavefronts, with n_{ref} denoting a reference refractive index, e.g. corresponding to freestream conditions. The optical wavefronts can be represented as isosurfaces of the OPL, i.e.,

$$\Lambda(\mathbf{x},t) = \text{const.} \,, \tag{4}$$

as indicated schematically in figure 1. As long as the flow speeds are small relative to the speed of light, and the propagation distances are small enough for light to propagate

through the flow before it has evolved, it is sufficient to think of the OPL integral in equation 1 as involving only the spatial structure of the refractive-index field, at each instant in time.

As the optical wavefronts propagate through the nonuniform refractive-index field $n(\mathbf{x}, t)$, the aerooptical interactions physically occur across the refractive fluid interfaces. These are the interfaces on which the refractive index n is constant. It is important to understand the role of these interfaces. While these fluid interfaces correspond to isosurfaces of the refractive-index field, i.e.,

$$n(\mathbf{x}, t) \;=\; \text{const.}\,, \tag{5}$$

it is crucial to recognize that the refractive-fluid interfaces will have a physical thickness whereas the refractive-fluid isosurfaces are geometrical objects with zero thickness. It is the physical thickness of the interfaces that is very important in aerooptics. We can introduce the local *interfacial thickness* h_n, defined per unit n, as the inverse of the refractive-index gradient magnitude, i.e.,

$$h_n(\mathbf{x}, t) \;\equiv\; \frac{1}{|\nabla n|} \tag{6}$$

[11] (Catrakis & Aguirre 2002). The distance between two neighboring isosurfaces, corresponding to n and $n + \mathrm{d}n$, will be $h_n\,\mathrm{d}n$. This is shown schematically in figure 2, for a single interface, and in figure 3 for several neighboring interfaces. We can distinguish between the general case, where the gradient magnitude is nonzero, i.e. $|\nabla n| > 0$, and the special case of zero gradient magnitude, i.e. $|\nabla n| = 0$, which will be discussed below. In regions of relatively-large refractive-index gradients, the isosurfaces are closely spaced and the interfaces are associated with a relatively-small thickness. In regions of weak refractive-index gradients, the isosurfaces will be located further apart and the interfaces will be relatively thicker. The interfacial thickness can be expected to be highly nonuniform at large Reynolds numbers. This is because of the strongly-intermittent character of fully-developed turbulent flows which becomes more intermittent with increasing Reynolds number for both incompressible and compressible flows (e.g. [12] Sreenivasan 1991, and references therein; [8] Smits & Dussauge 1996). As discussed by Jumper & Fitzgerald (2001 [3]), refractive-index fluctuations can arise in pure fluids, e.g. where density fluctuations are induced by temperature variations in low-speed air flows (e.g. [13] Jumper & Hugo 1995) or density fluctuations in compressible air flows (e.g. [14] Fitzgerald & Jumper 2000), or in mixtures of dissimilar fluids (e.g. [15] Brown & Roshko 1974; [7] Dimotakis, Catrakis, & Fourguette 2001). In all these different cases, the thickness of the refractive interfaces can be defined in the same manner, i.e. using equation 6.

Is the interfacial thickness finite? Is it nonzero? In turbulent flows, the interfacial thickness can be expected to be both nonzero and finite, in general, on physical grounds. The thickness must be nonzero wherever the local refractive-index gradient magnitude $|\nabla n(\mathbf{x}, t)|$ is finite, as indicated from equation 6. Only an infinite gradient can lead to a zero interfacial thickness. Physically, it is clear that for flows of real fluids, even at large but finite Reynolds numbers, the finite molecular diffusivities of the fluid ensure finite gradients and therefore finite interfacial thicknesses. A related observation, also indicated

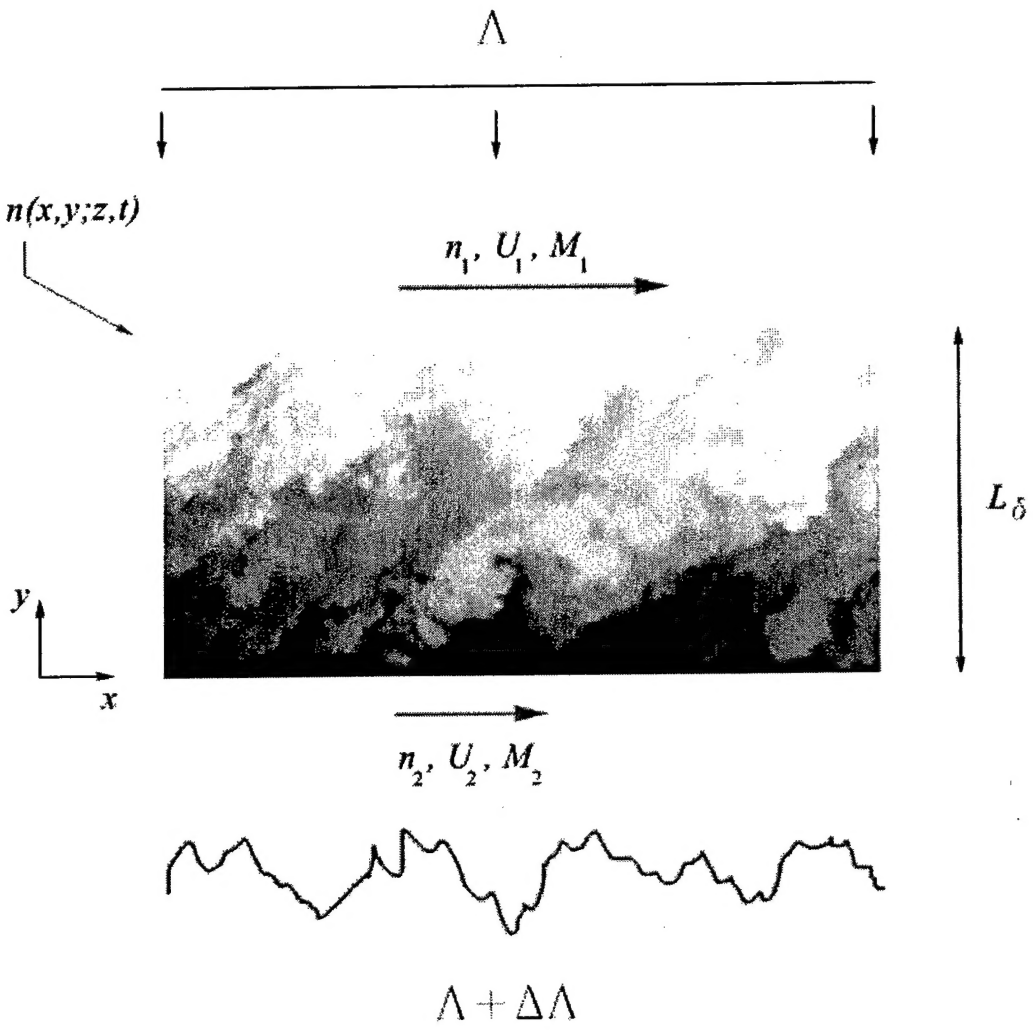

Figure 1: Schematic of a refractive-index field $n(x, y; z, t)$ at high compressibility, shown as the gray-level image at the inset, a planar incident optical wavefront with OPL Λ, and a propagated irregular optical wavefront with OPL $\Lambda + \Delta\Lambda$. L_δ is the large-scale transverse extent of the flow and measures the extent of the outer edges of the refractive fluid interfaces.

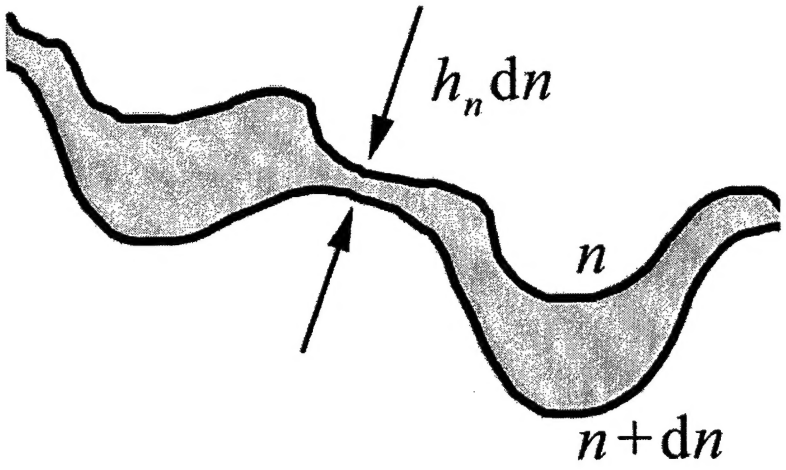

Figure 2: Schematic representation of a refractive interface, its interfacial thickness $h_n(\mathbf{x},t)$, and two neighboring isosurfaces of the refractive-index field $n(\mathbf{x},t)$.

from equation 6, is that the thickness must be finite as long as the gradient magnitude is nonzero. If the gradient is zero, which would correspond to a region of exactly-uniform refractive index, the thickness would be infinite in the context of equation 6 and one then must interpret the (infinity-times-zero) product $h_n\,\mathrm{d}n$ as a Dirac delta function whose integral becomes the distance given by the extent of the uniform-index region in the direction of the optical-ray propagation. In summary, we can expect physically that the interfacial thickness must be finite as long as the gradient is finite, consistent with equation 6. The thickness is an interfacial property, therefore, that has to be taken into account.

Since each optical ray physically propagates through refractive interfaces, one can intuitively expect that the local interfacial thickness should determine, at least in part, the local contribution to the OPL. Can this be seen in the OPL integral in equation 3? This can be done by rewriting equation 3, from the point of view of the refractive fluid interfaces, as

$$\Lambda(\mathbf{x},t) \;\equiv\; \int_{\mathrm{ray}} n(\ell,t)\; h_{n,\ell}\; |\mathrm{d}n|\,, \tag{7}$$

where the integration is now performed with respect to the refractive index n, rather than with respect to the spatial distance ℓ, and $h_{n,\ell}$ is the *effective interfacial thickness* defined as the component of the interfacial thickness in the direction of optical propagation, given by

$$h_{n,\ell} \;=\; \frac{1}{|\nabla n|_\ell}\,, \tag{8}$$

with $|\nabla n|_\ell$ denoting the effective gradient magnitude, i.e. the magnitude of the component of the local refractive-index gradient in the ℓ direction, *i.e.* in the direction of the optical-ray propagation. The component of the refractive-index gradient in equation 7

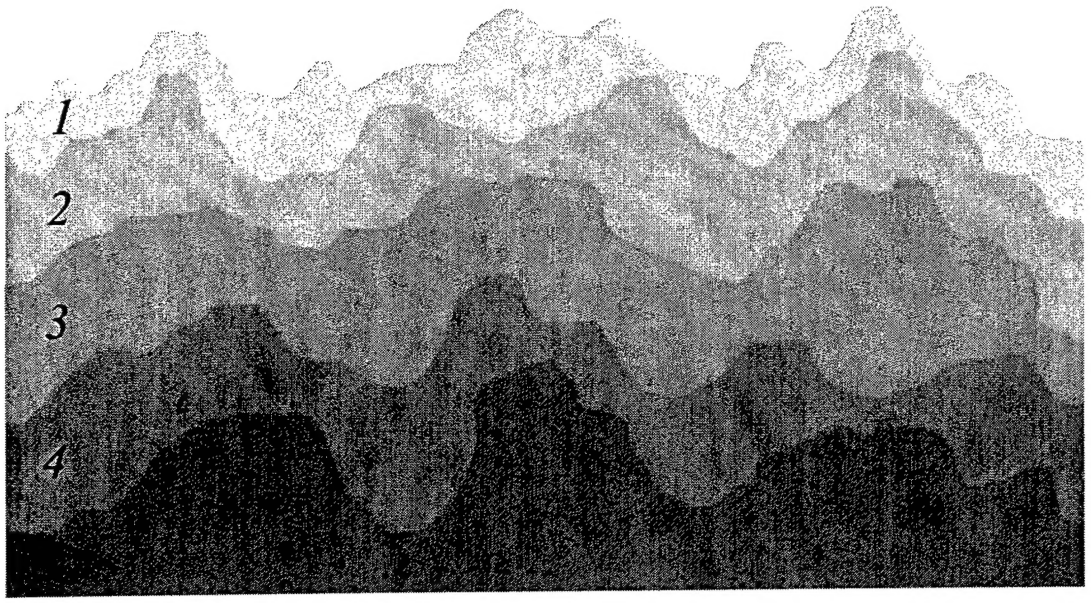

Figure 3: Schematic of several refractive fluid interfaces and the variability in interfacial thickness.

is,

$$|\nabla n|_\ell \equiv \frac{|\mathrm{d}n|}{\mathrm{d}\ell}, \tag{9}$$

as required, of course, in order for equations 2 and 6 to be consistent. Since the refractive index n could be locally increasing or decreasing as the light rays propagate, it is necessary to express the differential of n as the absolute-valued differential $|\mathrm{d}n|$, in equation 8. For interfaces locally normal to the optical rays, the gradient component $|\nabla n|_\ell$ has magnitude identical to the magnitude of $|\nabla n|$. Where the interfaces are locally not perpendicular to the optical rays, this component will be of smaller magnitude than $|\nabla n|$ and the effective interfacial thickness will be larger. In other words, the effective gradient is always *less than or equal to* the full gradient, i.e.

$$|\nabla n|_\ell \equiv |\nabla n|\,|\cos\theta| \leq |\nabla n|, \tag{10}$$

and the effective interfacial thickness is always *greater than or equal to* the full interfacial thickness, i.e.

$$h_{n,\ell} = \frac{1}{|\nabla n|_\ell} \equiv h_n\,|\sec\theta| \geq h_n, \tag{11}$$

where the angle θ, taken as $-\pi < \theta \leq \pi$, quantifies the interfacial orientation relative to the optical-propagation direction. These are important considerations as they can be used to develop a modeling approach based on the interfacial thickness, described below. As long as the refractive-index gradient magnitude is not zero, i.e. as long as $|\nabla n| > 0$, we can define θ as the angle between the refractive-index gradient vector and the local optical-ray propagation vector. The refractive-index gradient vector is always normal to

the local refractive interface. Combining equations 11 and 7, and writing again equation 7 for clarity, we see that the OPL integral of equation 3 can be expressed directly in terms of the interfacial-thickness variations along the optical propagation path as,

$$\Lambda(\mathbf{x},t) \equiv \int_{\text{ray}} n(\ell,t)\ h_n\,|\sec\theta|\ |\mathrm{d}n| = \int_{\text{ray}} n(\ell,t)\ h_{n,\ell}\ |\mathrm{d}n|\,, \tag{12}$$

where the first integral is in terms of the thickness h_n and relative orientation θ of the refractive interfaces, and the second integral is in terms of the effective interfacial thickness $h_{n,\ell}$. As mentioned above, in the context of the interfacial thickness in equation 5, these integrals require that $|\nabla n| \neq 0$. In those regions where $|\nabla n| = 0$, i.e. in regions of uniform refractive index, the (infinity-time-zero) product $h_n\,\mathrm{d}n$ must be interpreted again as a Dirac delta function whose integral is the distance, say $\Delta\ell$, corresponding to the extent of the uniform-index region in the optical-propagation direction, so that the contribution to the OPL integral becomes $\Delta\Lambda = n\,\Delta\ell$. We note that, in uniform-index regions, the interfacial orientation θ has no meaning and is not needed. In those instances where the fluid interface happens to be locally tangent to the optical-propagation direction, i.e. if $\theta = \pm\pi/2$, the term $|\sec\theta|$ will be infinite but in such cases the refractive index will locally be uniform since the interface will be aligned with the optical-propagation direction, i.e. $|dn| = 0$ in such cases. In those cases, therefore, the contribution to the OPL integral will again be $\Delta\Lambda = n\,\Delta\ell$ with $\Delta\ell$ identified as the length of the interface that is tangential to the optical-propagation direction. We should also note that, in general, one may also need to take into account other possibilities such as total internal reflection or the development of caustics. These possibilities depend on the magnitudes of refractive gradients, and relative interfacial orientations, encountered in practice.

In summary, the proposed interfacial-thickness approach is based on relating the OPL to the interfacial-thickness variations. Whereas the integral in equation 3 is conducted over space, the integrals in equations 7 and 12 are expressed as integrals over the refractive index and are useful to determine the manner in which the refractive interfaces physically contribute to the OPL. In addition to the local refractive index n, equation 11 shows that the OPL variations arise from the variability in the interfacial thickness h_n and the fluctuations in the interfacial orientation θ, or the variations in the effective interfacial thickness $h_{n,\ell}$. Knowledge of the variability in the effective interfacial thickness, and its relation to the flow dynamics, can be expected therefore to provide physical insight into the relation between the OPL behavior and the interfacial structure.

We have decided to demonstrate the use of the interfacial-thickness approach on turbulent high-compressibility fluid interfaces. We have chosen to examine the applicability of the proposed approach to high-compressibility fluid interfaces in order to develop a large-scale aerooptics modeling methodology useful for high-compressibility flow conditions. There are available large-scale aerooptics modeling methods that have successfully addressed weakly-compressible flows (e.g. [3] Jumper & Fitzgerald 2001) and incompressible flows (e.g. [5] Truman & Lee 1990; [16] Chew & Christiansen 1991; [7] Dimotakis, Catrakis, & Fourguette 2001). These methods are essentially based on the Brown-Roshko large-scale organized-structure approach ([15] Brown & Roshko 1974) with direct extensions to weakly-compressible flows, and will be discussed briefly below. It is known, however, that high-compressibility turbulent flows exhibit significant differences compared

to weakly-compressible or incompressible flows (e.g. [17] Papamoschou & Roshko 1988; [18] Papamoschou 1991; [19] Clemens & Mungal 1995). A more general approach is desirable, to be able to address aerooptical effects across the full range of compressibilities, and it is toward this goal that the interfacial-thickness approach can be particularly useful.

Figure 4a shows an example of a two-dimensional spatial streamwise slice of the refractive-index field in a shear layer between optically-different gases, with convective Mach number $M_c \sim 1$ and Reynolds number $Re \sim 10^6$ based on the large-scale extent L_δ of the flow ([7] Dimotakis, Catrakis, & Fourguette 2001). Also shown is an example of a low-compressibility ($M_c \sim 0.2$) shear-layer image in figure 4b, for comparison. These flow images span the entire large-scale transverse extent of the flow and, although not fully resolved, they capture a relatively-wide range of scales ($\sim 500 : 1$) which permits a study of the large-scale behavior. It should be noted that the refractive-index field in figure 4a reflects effects of both compressibility and mixing, as a result of the use of optically-different gases, and may not directly represent the density-field behavior, as has been discussed by Jumper & Fitzgerald (2001 [3]). The data in figure 4a, however, make possible an examination of the interfacial-thickness approach at high levels of compressibility. Density-field variations, in turbulent compressible flows, can be expected to exhibit features attributable to vortical structures at various scales, compression-wave regions (e.g. shocklets), and expansion-wave regions. The refractive-index field in figure 4a reflects these flow mechanisms, albeit indirectly, and provides the opportunity to examine the role of high-compressibility fluid interfaces and in particular their physical thickness in generating the aerooptical distortions.

The interfacial-thickness fields, h_n, corresponding to the refractive-index fields, n of figures 4a and b, are shown in figures 5a and b. The interfacial thickness was computed by first evaluating the refractive-index gradient magnitude $|\nabla n|$ and subsequently computing its inverse ([20] Aguirre, Catrakis, & Ruiz-Plancarte 2003), according to the interfacial-thickness definition in equation 6. The local refractive-gradient magnitudes, and interfacial thicknesses, are necessarily under-/over-estimated respectively because the images are not fully resolved. The computed gradients and thicknesses are essentially coarse-grained values at the image-resolution scale. However, these values permit the *relative spatial variations* to be examined and this is what is needed in the present context. Since the refractive-index data of figures 5a and b are from two-dimensional slices of the flow, only two of the three spatial refractive-index derivatives necessary to evaluate the full gradient magnitude can be computed. The interfacial-thickness fields in figures 5a and b thus corresponds to the in-plane refractive-index gradient magnitude. We note, however, that only the component of the full gradient, or interfacial thickness, along the optical-ray propagation direction is needed, as is evident in equations 9, 10, and 11. In other words, even if the full gradient were available, one would compute the component of it in the optical-propagation direction and this would be equivalent to using the in-plane component in addition to the in-plane interfacial orientation, for optical wavefronts propagating in the plane of the flow shown in figures 5a and b, or figures 4a and b. In figures 5a and b, the in-plane gradient magnitudes are shown such that darker regions denote higher values of the gradient magnitude. Since the in-plane interfacial thickness is the inverse

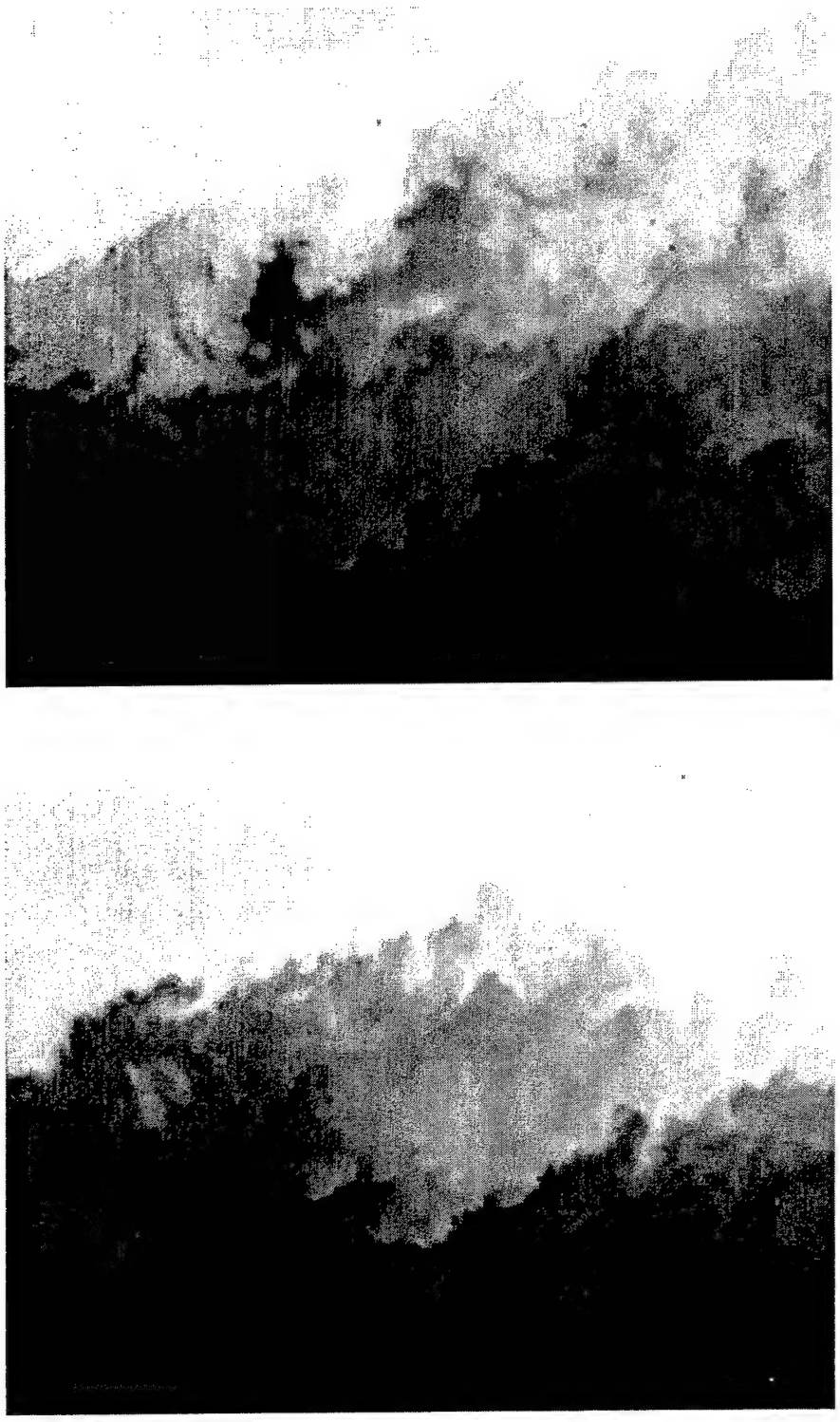

Figure 4: (a) (Top) Refractive-index field in a streamwise slice of a high-compressibility ($M_c \sim 1$) large-Reynolds-number ($Re \sim 10^6$) shear layer between optically-different gases [7]. (b) (Bottom) Low-compressibility ($M_c \sim 0.2$) shear-layer refractive field [7].

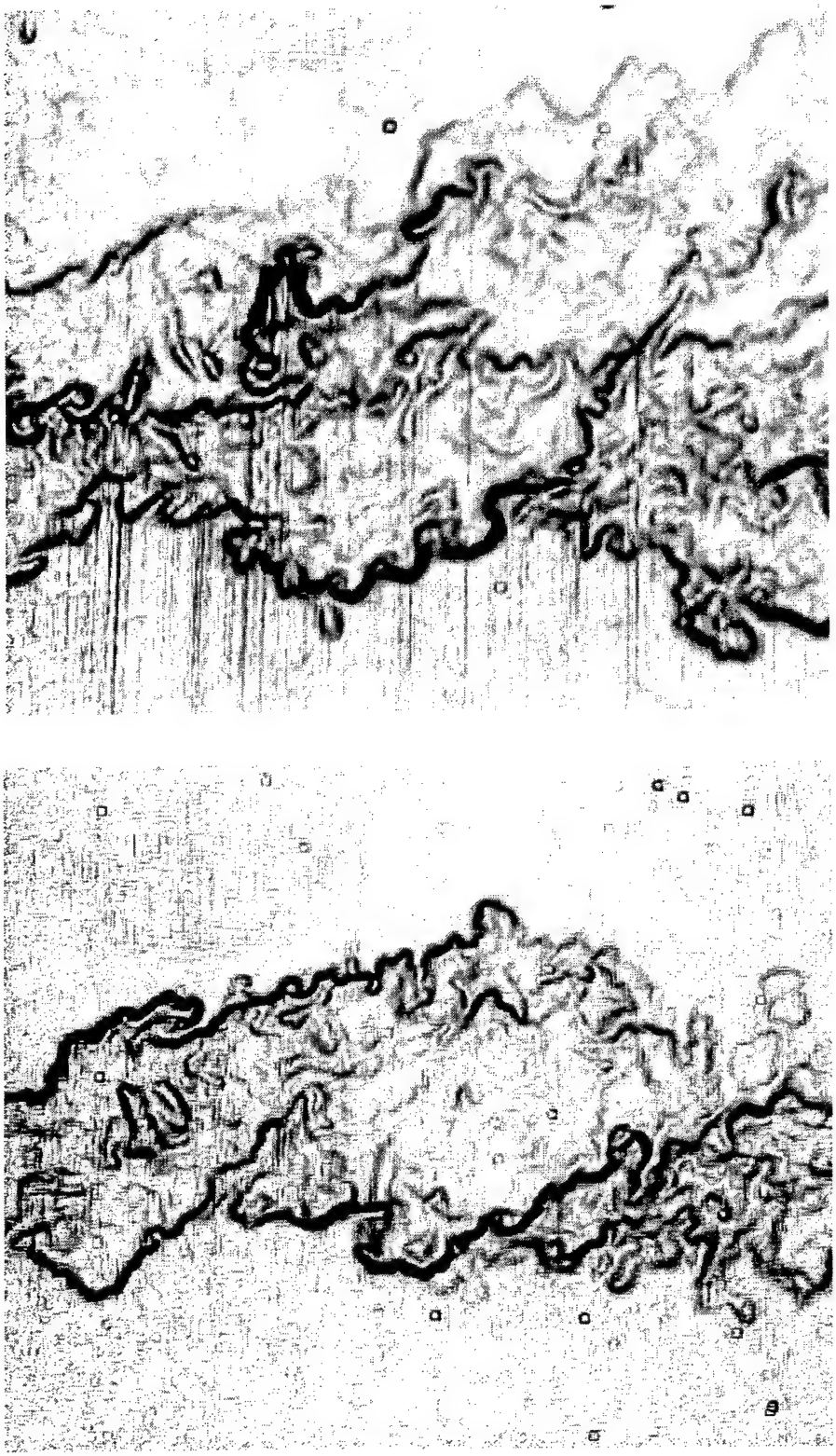

Figure 5: (a) (Top) Interfacial-thickness field h_n at high compressibility corresponding to the refractive-index field of figure 4. Darker regions denote thinner interfaces, i.e. the dark regions correspond to the high-gradient interfaces. (b) (Bottom) Low-compressibility interfacial-thickness field.

of the in-plane gradient magnitude, the darker regions denote locally-thin high-gradient interfaces. Also evident in figures 5a and b are the variations in the interfacial orientation. Depending on the direction of optical beam propagation, the relative interfacial orientation θ will be different along the beam-propagation path. Figures 5a and b indicate, however, that the interfacial orientation is sufficiently irregular that, at least locally, there is a wide distribution of interfacial directions. It is important to recall the meaning of equations 10 and 11, i.e. that interfaces of a given thickness will have an effective thickness that is always *greater than or equal to* it for any optical-beam propagation direction. In other words, a given gradient magnitude will result in an effective gradient magnitude that is always *smaller than or equal to* it, irrespective of the optical-beam propagation direction. If one identifies, therefore, the regions of high-gradient interfaces in the flow, then there can be no effective gradient magnitudes that are higher yet.

Four significant observations can be made, at high compressibility, on the basis of figure 5a and other interfacial-thickness fields at the same flow conditions:

(a) *the high-gradient regions occupy a relatively-small part of the turbulent shear-flow region,*

(b) *the high-gradient regions are sheet-like and can be thought of as high-gradient interfaces,*

(c) *the high-gradient interfaces exist at various transverse locations in the shear-flow region,* and

(d) *the refractive-index gradient magnitude exhibits variations along the high-gradient interfaces.*

It is important to note that these observations refer to the *instantaneous* spatial structure of the interfacial-thickness field, and this is practically very relevant for aerooptics since it is the instantaneous flow structure that needs to be understood, modeled, and controlled. The ensemble-averaged behavior can be expected to be quite different, in particular simpler with less irregular ensemble-averaged interfaces, and we hope that this will be addressed in future studies, in order to compare the average behavior to the instantaneous behavior examined here.

Observation (a) refers to the fact that the high-gradient regions are spatially relatively isolated, as is evident in figure 5a. In other words, *large parts of the instantaneous flow region have relatively low refractive-gradient magnitudes.* The high-gradient regions appear to occupy only a small fraction of the flow region. This is consistent with computational results at low Reynolds numbers in studies by Samtaney, Pullin, & Kosović (2001 [21]) who found that regions of high gradient magnitudes in isotropic and homogeneous turbulence occupy a relatively-small fraction of the flow.

Observation (b) indicates, further, that the high-gradient regions are not only spatially isolated but are sheet-like, i.e. these regions are confined to thin layers in the turbulent-flow region. These high-gradient regions can be thought of physically, therefore, as

locally-thin interfaces. Sheet-like structure, in three-dimensional space, is consistent with the string-like structure evident in the two-dimensional spatial images or slices such as figure 5a.

Observation (c) is particularly important because it illustrates a major qualitative difference between high-compressibility flows and weakly-compressible flows. The data indicate that the high-gradient interfaces, although spatially isolated and occupying a relatively small fraction of the flow region, are present at *several different transverse locations in the instantaneous flow structure*, as is evident in the high-compressibility interfacial-thickness field of figure 5a and in direct contrast to the low-compressibility interfacial-thickness field of figure 5b. Whereas at low compressibility, the high-gradient interfaces are mostly confined to the instantaneous outer edges of the flow, it is clear that at high compressibility the high-gradient interfaces can be found both in the interior and near the outer boundaries in instantaneous realizations of the flow. This is in sharp contrast with the behavior in low-compressibility turbulent shear flows ([5] Truman & Lee 1990; [7] Dimotakis, Catrakis, & Fourguette 2001), cf. the interfacial-thickness behavior in figure 5b, where isolated high-gradient regions are not found in the interior of the flow, as a result of large-scale organized structures which confine such interfaces mostly to the outer parts of the shear region. At the high-compressibility flow conditions examined presently in figure 5a, the high-gradient interfaces are clearly not confined to the outer boundaries of the flow and are not excluded from the interior of the flow.

Observation (d) is also important because it indicates that, on the high-gradient interfaces, the refractive-index gradient is not constant, i.e. it fluctuates along these interfaces. This must be taken into account if one wishes to model the aerooptical effects of these interfaces, and this will be addressed in the proposed modeling approach below. We note that the variability of the thickness along the high-gradient interfaces is attributable to both intermittency effects associated with the large Reynolds number and the presence of compact shocklets associated with the high compressibility of the flow.

These observations, and the dramatic difference between the high-compressibility behavior and the low-compressibility behavior, are illustrated also in figures 6a and b. The observation, at high compressibility, that the high-gradient regions are spatially isolated even though they occupy several transverse locations in the flow, and the interpretation of the optical wavefront phase in terms of the interfacial thickness variations, indicate that these isolated regions are the dominant elements for the large-scale optical distortions at high compressibility. While the low-gradient regions are of wide transverse extent, and therefore do contribute to the OPL integral, it is the structure of the high-gradient (locally-thin) interfaces that can form the basis of a description that captures the large-scale optical distortions, as explained in the modeling approach we have proposed which is described below.

The observations of the instantaneous structure of the interfacial-thickness field and the interpretation of the OPL in terms of the interfacial-thickness variations can be used to develop a modeling methodology that is useful for capturing the large-scale optical distortions at high compressibility. Before describing the proposed modeling approach, it is helpful to recall the previous work in incompressible and weakly-compressible shear

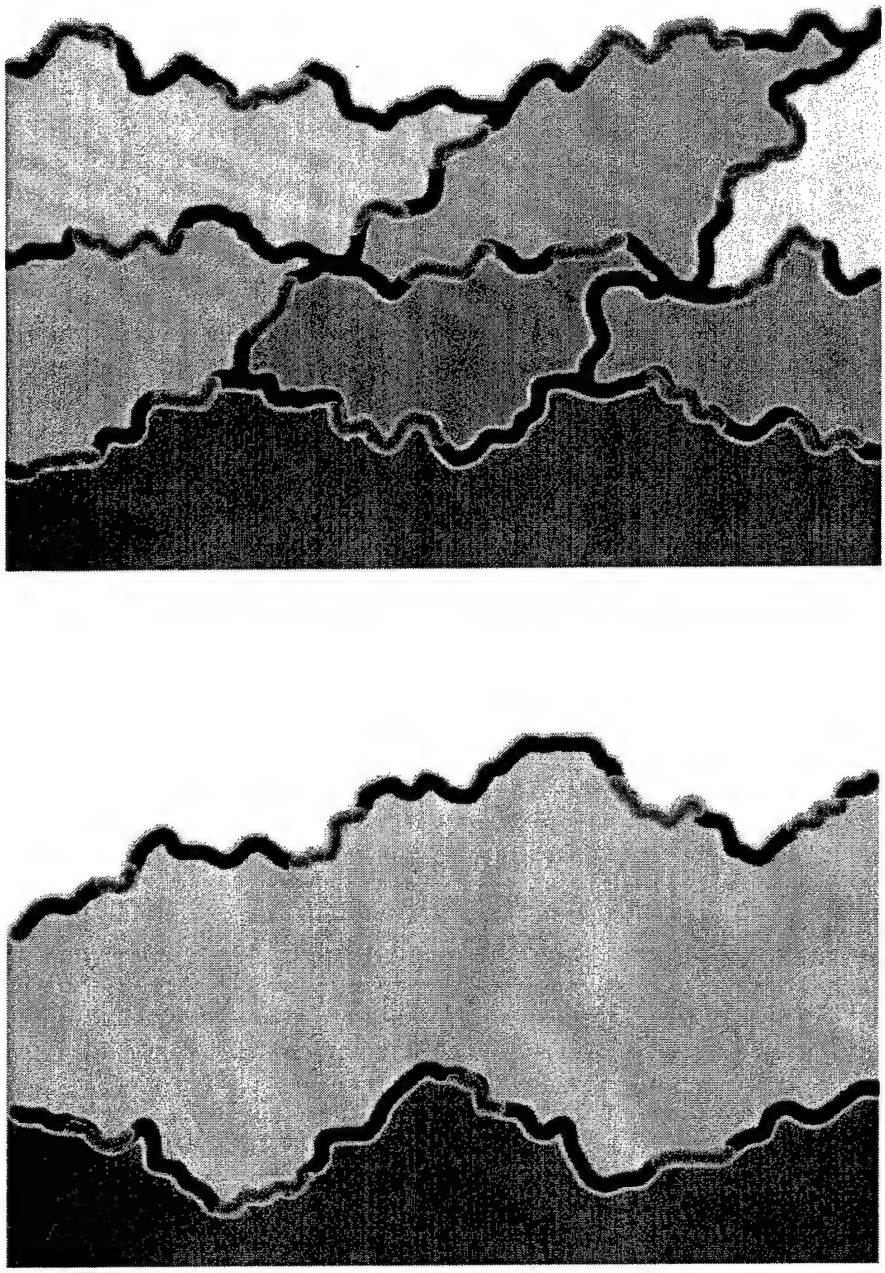

Figure 6: (a) (Top) Schematic of network of spatially-isolated high-gradient interfaces at high compressibility. Darker regions denote higher gradients or locally-thinner interfaces. (b) Schematic of high-gradient interfaces at low compressibility.

layers that has been successful in modeling the large-scale aerooptical distortions. In the case of incompressible shear layers of dissimilar gases, the Brown-Roshko vortical structures ([15] Brown & Roshko 1974) generate large-scale regions of nearly-uniform refractive index and this enables the use of the outer interfaces to model the large-scale optical distortions ([7] Dimotakis, Catrakis, & Fourguette 2001). In the case of weakly-compressible shear layers, there are large-scale regions of reduced density and pressure in the flow as shown by Fitzgerald & Jumper (2000 [14]). These large-scale reduced-density regions are essentially weakly-compressible analogues of the Brown-Roshko structures. Jumper & Fitzgerald (2001 [3]) have developed a model based on these large-scale low-density regions, or density "wells", and have shown that it is able to reproduce well the large-scale optical distortions at low compressibility.

It is known, however, from various investigations of high-compressibility flows, that there is a strong qualitative difference between the structure of weakly-compressible flows and high-compressibility flows (e.g. [22] Bogdanoff 1983; [17] Papamoschou & Roshko 1988; [18] Papamoschou 1991; [23] Samimy & Elliott 1990; [24] Samimy, Reeder, & Elliott 1992; [19] Clemens & Mungal 1995). For shear layers, in addition to the well-known reduction in the growth rate there is a major difference in the organization of the flow and in particular in the internal structure of the flow as the compressibility level is increase. In particular, accepting the convective Mach number M_c as an appropriate measure of compressibility,

$$M_c \equiv \frac{U_1 - U_2}{a_1 + a_2}, \tag{13}$$

where $U_{1,2}$ and $a_{1,2}$ denote the freestream speeds and sound speeds, respectively, there is evidence that the flow behavior transitions and changes dramatically at convective Mach numbers above a certain value ([19] Clemens & Mungal 1995). Specifically, in the range

$$M_c \gtrsim 0.6, \tag{14}$$

which corresponds to high compressibility according to most available data, the turbulent flow structure and fluid interfaces appear to be substantially more irregular, and in a fundamentally-different way, compared to the behavior at low compressibility.

Comparison of the images in figures 5a and b, example, indicates that high-compressibility shear layers exhibit *multiple* regions spanning different transverse locations where the refractive-index gradients are relatively weak. At the boundaries between these multiple regions, the high-gradient interfaces reside. As discussed above, these high-gradient interfaces appear to form a highly-irregular network in the flow. Is there a way to model the interfacial-thickness field at high compressibility in order to reproduce the aerooptical distortions? In particular, how can the large-scale optical distortions be modeled at high compressibility and which part of the interfacial-thickness structure is necessary to capture the large-scale optical distortions?

Our proposed modeling approach, at high compressibility, is based on the crucial observation above that the high-gradient interfaces, although located at various transverse locations, are *spatially isolated*, cf. figures 5a and 6a. Because the high-gradient interfaces occupy a relatively-small fraction of the total turbulent-flow region, we can develop a

modeling approach with these interfaces as the dominant elements. A gradient-magnitude threshold is first chosen in order to identify the high-gradient interfaces. We note that it is crucial to retain the high-gradient interfaces. It may appear, at first sight, that these high-gradient interfaces could be neglected since they only occupy a small fraction of the turbulent-flow region. On the contrary, the high-gradient interfaces contribute significantly to the OPL integral because, even though the thickness $h_{n,l}$ is relatively small, the differential $|\mathrm{d}n|$ is relatively large across such interfaces. Significantly, there is no way to *avoid* including these high-gradient interfaces in the modeling approach. Fortunately, however, it is precisely because these interfaces are spatially isolated that it is feasible to approximate the regions in between these interfaces as zero-gradient regions, i.e. as uniform-index regions. This raises the important question of how to propagate the beam, in the model, through these regions. For comparison, in the Dimotakis, Catrakis, & Fourguette (2001 [7]) modeling approach, the refractive index in the large-scale regions bounded by the outer interfaces is modeled on the basis of the value predicted from the large-scale entrainment. For the present case of high compressibility, however, there are multiple regions through which the beam must be propagated. We propose that the way to do this is to use the *gradient information* along the high-gradient interfaces to update the refractive index as the OPL integral is computed across these interfaces. The *locations* of the high-gradient interfaces provide the length scales needed to propagate the beam through the regions in between the interfaces. The proposed modeling approach can be summarized therefore in four steps:

(a) *the high-gradient interfaces are first identified, including their spatial location and gradient values,*

(b) *the optical beam is propagated across the high-gradient interfaces by updating the OPL integral using the gradient values at these interfaces,*

(c) *the regions in between the high-gradient interfaces are modeled as zero-gradient regions*, and,

(d) *the value of the refractive index in each zero-gradient region, between the high-gradient interfaces, is computed using the gradient value on the interface which the beam propagates across as it enters each zero-gradient region.*

A schematic illustrating the basic idea of this model is shown in figure 7 for the high-compressibility case. The multiple regions in the interior of the flow are denoted as B through G. We emphasize that it is important, and necessary, to retain both the *location of* and *gradient values along* the high-gradient interfaces in the proposed modeling approach.

The utility of this approach can be demonstrated with the high-compressibility interfacial-thickness data. Figure 8 shows a modeled interfacial-thickness field where $\sim 50\%$ *of the refractive-gradient magnitudes have been set to zero*, compared to the original field in figure 5a. The OPL integral was computed using this modeled interfacial-thickness field by following the above four steps. The comparison between the full aerooptical-wavefront OPL (solid curve) and the modeled OPL (dashed curve) in shown in figure 9. Good

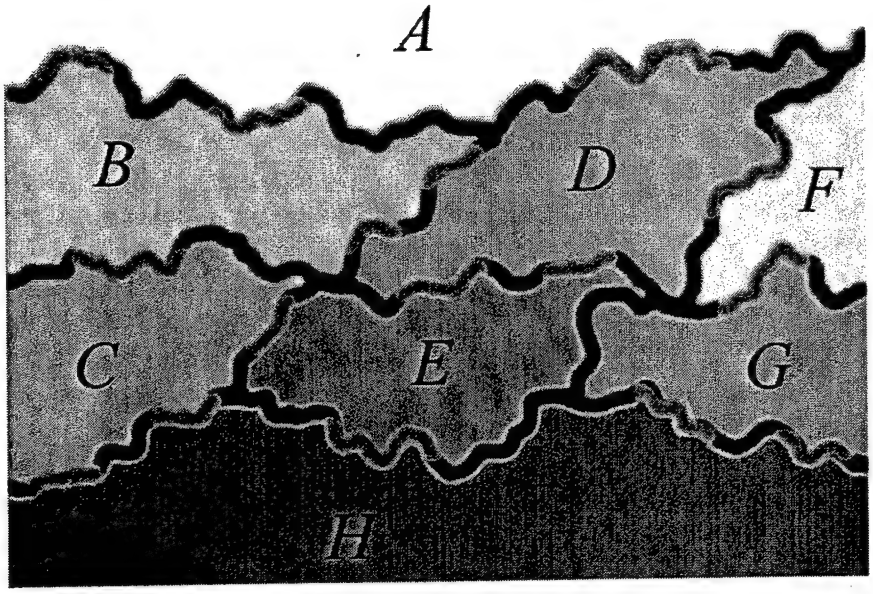

Figure 7: The labeled regions in the interior of the flow, i.e. regions B through G, correspond to the low-gradient regions at high compressibility. In the proposed modeling approach, the high-gradient interfaces, or boundaries between the low-gradient regions, are treated as the dominant elements necessary to model the large-scale optical distortions at high compressibility.

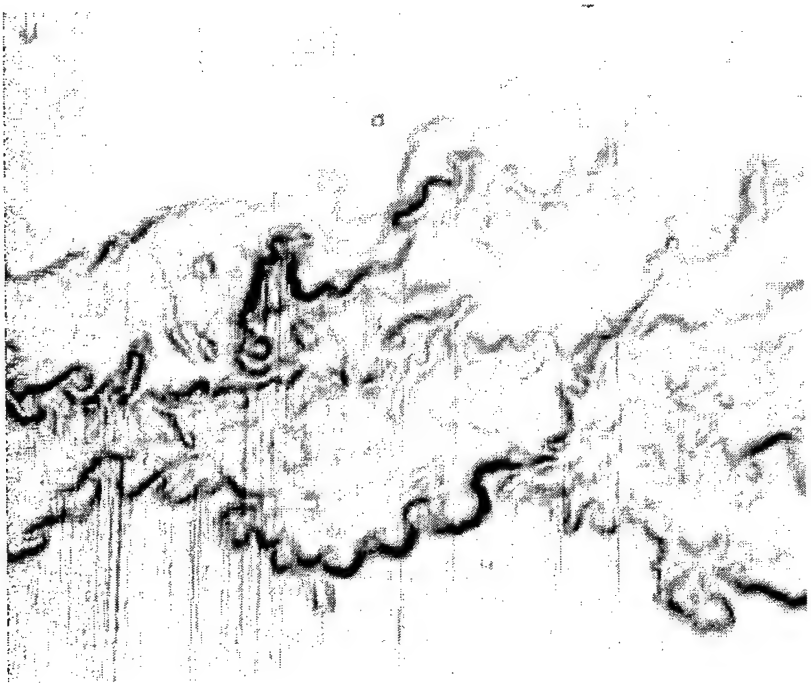

Figure 8: Modeled interfacial-thickness field, with $\sim$ 50% of the gradient magnitudes neglected, at high compressibility, cf. figure 5a.

agreement is evident in terms of the large-scale OPL variations. This shows that the proposed modeling approach can be used to reproduce the large-scale optical distortions at high compressibility, in a shear layer, using the high-gradient information. Instead of the full interfacial-thickness field, information on the high-gradient interfaces only appears to be sufficient to model the large-scale aerooptical distortions. The location of the high-gradient interfaces and the value of the gradient across (or of the thickness of) these interfaces is enough to capture the dominant contributions that generate the large-scale aerooptical distortions. The optical wavefronts are propagated through the high-gradient (locally-thin) interfaces and the gradient value across these interfaces is used to compute the difference in the optical path length, while in the low-gradient regions between the high-gradient interfaces the wavefronts are propagated neglecting the presence of the low gradients, i.e. as if those regions are zero-gradient regions. The high-gradient interfaces, in this example, are identified in an absolute sense, i.e. by thresholding the entire instantaneous gradient field. A further refinement, potentially, could be envisaged by retaining those interfaces that have high gradients *relative to* their neighboring interfaces. The proposed modeling approach offers a reduction in the amount of flow information needed to capture the large-scale aerooptical distortions at high compressibility.

In summary, the new interfacial-thickness approach has been proposed to examine optical-wavefront propagation through turbulent flows in terms of the variability in the physical thickness of the refractive fluid interfaces. The interfacial thickness is given by the inverse of the refractive-index gradient magnitude. As long as the gradient magnitude is finite, the interfacial thickness is also finite. The thickness can be highly variable at large Reynolds numbers and high compressibility. The interfacial thickness plays an important role in aerooptics as indicated by expressing directly the optical path length (OPL) in terms of the interfacial-thickness variations. Demonstration of this approach on refractive-field data in shear layers at high compressibility ($M_c \sim 1$) and large Reynolds number ($Re \sim 10^6$) reveals that regions of high refractive-gradient magnitudes are located at various transverse locations in the flow, i.e. both in the interior and near the outer boundaries, and form highly-irregular networks. Significantly, the high-gradient regions are found to be spatially isolated, i.e. occupy a relatively-small fraction of the shear layer. This observation, coupled with the interpretation of the OPL in terms of interfacial-thickness variations, are utilized to propose and demonstrate a new modeling approach where the high-gradient interfaces are the dominant elements necessary to reproduce the large-scale optical distortions at high compressibility. Both the location of and the gradient values along the high-gradient interfaces are utilized in this modeling approach. A reduction of $\sim 50\%$ in the amount of interfacial information needed is shown to reproduce well the large-scale optical distortions at high compressibility. The present results suggest applicability of the proposed approach to other high-compressibility flows, by modeling the large-scale optical distortions in terms of the structure of the high-gradient interfaces. The proposed approach can be expected to be useful in studies of the dynamics of aerooptical interactions at high compressibility (e.g. [25] Thurow, Samimy, Lempert, Harris, Widiker, & Duncan 2003), in computational modeling and simulations of aerooptical interactions in high-speed flows (e.g. [26] Jones & Bender 2001), as well as in efforts to extend fluid-mechanical techniques that control or regularize aerooptical in-

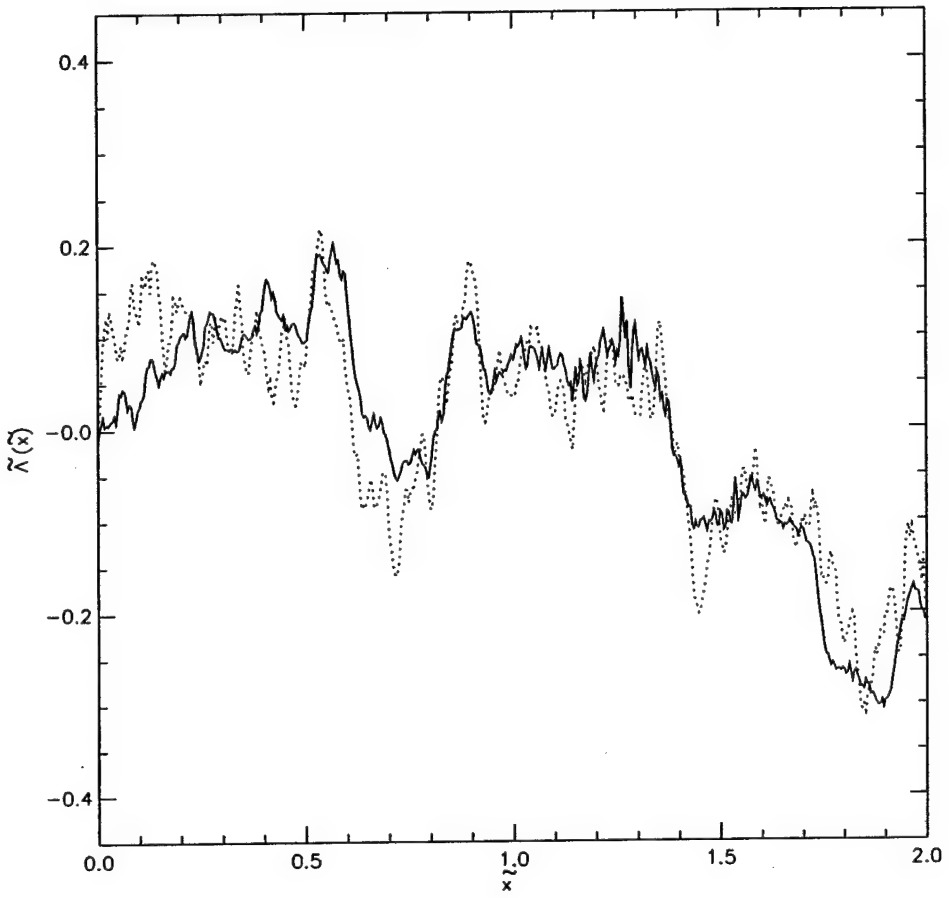

Figure 9: Comparison, at high compressibility, between the full wavefront OPL (solid curve) using the complete interfacial-thickness field (figure 5a), and the modeled OPL (dashed curve) using the high-gradient interfaces with $\sim 50\%$ of the gradient magnitudes neglected (figure 8). The spatial and OPL coordinates are normalized based on the large-scale flow extent L_δ. The large-scale optical distortions are reproducible, even with a $\sim 50\%$ reduction in interfacial information, demonstrating the use of the proposed interfacial-thickness modeling approach at high compressibility.

teractions in weakly-compressible flows (e.g. [27] Stanek, Sinha, Seiner, Pearce, & Jones 2002), [28] Siegenthaler, Jumper, & Asghar 2003) to higher compressibilities.

Aerooptical-wavefront anisotropy and small-scale structure at large Reynolds numbers and high compressibility:

The large-scale properties of aerooptical interactions in turbulent flows can be expected to be strongly dependent on the flow geometry and/or boundary conditions (e.g. [5] Truman & Lee 1990; [7] Dimotakis, Catrakis, & Fourguette 2001; [3] Jumper & Fitzgerald 2001). In contrast, at least at high Reynolds numbers and for incompressible flow conditions, there is evidence that the small-scale flow structure can exhibit scaling or self-similar behavior which is universal, or nearly universal, in the sense that the small-scale statistics of various types of turbulent interfaces appear to be independent of the flow geometry or large-scale behavior, to a good approximation (e.g. [12] Sreenivasan 1991; [29] Catrakis, Aguirre, & Ruiz-Plancarte 2002) as long as the Reynolds number is sufficiently large, i.e. corresponding to fully-developed turbulence (e.g. [30] Dimotakis 2000). For applications requiring high-resolution and/or long-range optical imaging or beam propagation, knowledge of the small-scale properties is needed in addition to the large-scale behavior.

A useful point of view in developing techniques to characterize turbulence-generated fluid interfaces is to quantify the physical structure of these interfaces in terms of their geometric properties such as the extent to which the interfaces exhibit self-similar or fractal behavior at small scales (e.g. Sreenivasan 1991). Since the structure of aerooptical wavefronts is determined by the turbulent flow structure, one may expect that the aerooptical distortions may exhibit self-similar behavior at small scales. This has been suggested theoretically for optical wavefronts distorted by incompressible turbulent flows (e.g. [31] Hentschel & Procaccia 1983; [32] Schwartz, Baum, & Ribak 1993; [33] Schwartz, Baum, & Ribak 1994). For compressible flows, there is some evidence that the small-scale structure of fluid interfaces can exhibit self-similarity (e.g. Sreenivasan & Johnson (1989) & Poggie (1991), cited in [8] Smits & Dussauge 1996, p. 250). Such self-similarity would be expected to be at most weakly dependent on the large-scale flow properties as far as the statistics of the instantaneous interfaces are concerned. Thus, for compressible turbulence, one might expect self-similar scaling behavior for the small-scale properties of both the turbulent fluid interfaces and the turbulence-distorted optical wavefronts. Self-similar behavior of the optical wavefronts, if found at high compressibility, would permit extrapolating and predicting the small-scale optical behavior to the high Reynolds numbers of interest in practical applications at high-speed flight.

One of the practical and fundamental objectives in aerooptics is to develop the means to extrapolate the behavior of the optical-wavefront structure to larger Reynolds numbers, including effects of compressibility. Knowledge of the small-scale structure of aerooptical wavefronts is needed to achieve this. Optical wavefronts propagating through turbulent flows can be expected to exhibit behavior that is similar to, or related closely to, the flow structure. To be able to extrapolate the behavior of a turbulence-generated refractive-index field $n(\mathbf{x}, t)$ to large Reynolds numbers, it is important that the Reynolds number of the flow under study be at least above the minimum value associated with the transition

to fully-developed turbulence (e.g. [30] Dimotakis 2000), i.e.

$$Re \gtrsim 10^4 . \tag{15}$$

As long as the turbulent flow is fully developed, satisfying the criterion in equation 15, the range of scales exhibited by the refractive field $n(\mathbf{x}, t)$ increases with increasing Reynolds number as,

$$\frac{\lambda_{\text{max}}}{\lambda_{\text{min}}} \sim Re^{3/4} , \tag{16}$$

for gas-phase flows, where λ_{min} is the smallest scale or Kolmogorov scale and λ_{max} is the largest scale identified as the extent of the flow region through which the wavefronts propagate or alternatively as the extent of large-scale shear in the flow. The 3/4 exponent in equation 16 arises from the role of the energy dissipation rate and the viscosity in gas-phase flows in imposing a limit for the smallest flow scales ([34] Kolmogorov 1941; cf. also [35] Taylor 1935, and [36] Richardson 1922). An important aspect of large-Reynolds-number flows and refractive-index fields is that there is a wide range of scales bounded from above by λ_{max} and from below by λ_{min},

$$\lambda_{\text{min}} \ll \lambda \ll \lambda_{\text{max}} , \tag{17}$$

where similarity properties (e.g. [34] Kolmogorov 1941), including possibly self-similarity (e.g. [12] Sreenivasan 1991), are present. Such properties are important because they can be expected to provide the means to extrapolate the aerooptical behavior to the large Reynolds numbers encountered in practice, in both incompressible and compressible flows (e.g. [8] Smits & Dussauge 1996).

In order to characterize aerooptical distortions over the wide range of scales associated with large values of the Reynolds number (cf. equations 15-17), techniques are needed that enable the description of optical-wavefront structure as a function of scale. Most previous studies of the flow behavior and/or of the optical-wavefront behavior have focused on spectral descriptions (e.g. [7] Dimotakis, Catrakis, & Fourguette 2001) or equivalently on descriptions based on second-order structure functions (e.g. [37] Andrews & Phillips 1998). Spectral descriptions characterize the behavior in Fourier space, however, and do not uniquely identify the geometrical structure of the turbulent flow or optical wavefronts. This is because power spectra provide no phase information. The description of the geometrical structure of turbulent flows in physical space is a relatively-recent development (e.g. [12] Sreenivasan 1991; [29] Catrakis, Aguirre, & Ruiz-Plancarte 2002) and is based on box-counting techniques. A generalized version of the box-counting technique, that can characterize anisotropic surfaces such as optical wavefronts, will be proposed and described below. The issue of optical-wavefront anisotropy is first addressed as it is a crucial physical aspect of wavefront structure and an important ingredient of the new box-counting technique described below.

At the level of description of geometrical optics, the governing equation for the propagation of optical wavefronts is the eikonal equation for the optical path length (OPL) $\Lambda(\mathbf{x}, t)$ or, equivalently, the integral for the OPL in terms of the refractive index along the optical propagation path, i.e.

$$|\nabla \Lambda| = n , \quad \text{or} , \quad \Lambda(\mathbf{x}, t) \equiv \int_{\text{ray}} n(\ell, t) \, \mathrm{d}\ell \equiv \int_{\text{ray}} n(\ell, t) \, h_{n,\ell} \, |\mathrm{d}n| , \tag{18}$$

where the first integral is over the physical distance ℓ along the propagation path. In the second integral, the OPL is expressed directly in terms of the effective refractive-interface thickness $h_{n,\ell} = 1/|\nabla n|_\ell$ ([1] Catrakis & Aguirre 2003). The optical wavefronts are isosurfaces of the OPL, i.e.

$$\Lambda(\mathbf{x}, t) \;=\; \text{const.}\,, \tag{19}$$

and in turbulent flows, especially at large Reynolds numbers, the OPL isosurfaces can be highly irregular. In the present work, our objective is to characterize the physical structure of the optical wavefronts as a function of scale.

The first issue that needs to be addressed is that, physically, aerooptical wavefronts are highly-anisotropic surfaces. This is because optical wavefronts span spatial dimensions as well as the OPL dimension, and these can be of very different extent physically. This is especially so because the refractive-index variations, e.g. as quantified by the root-mean-square magnitude, are relatively small when compared to unity for gas-phase flows. Consequently, as the integrals in equation 4 suggest, the OPL variations are much smaller than the spatial transverse extent (i.e. aperture) of any optical beam in practice. In other words,

$$|\Delta n|_{\text{rms}} \;\ll\; 1\,, \quad \text{and}\,, \quad |\Delta\Lambda|_{\text{rms}} \;\ll\; |\Delta\ell|\,, \tag{20}$$

where $|\Delta_n|_{\text{rms}}$ and $|\Delta\Lambda|_{\text{rms}}$ denote respectively the root-mean-square magnitudes of the refractive-index variations and of the OPL variations of the distorted wavefront, and $|\Delta\ell|$ denotes a measure of the total optical-propagation path which is $|\Delta\ell| \sim L_\delta$, i.e. comparable to the large-scale extent L_δ of the flow, as far as the aerooptical interactions are concerned. This strong anisotropy of aerooptical wavefronts refers to their physical, unnormalized structure. One may normalize the OPL so that the effective degree of anisotropy can change. By also scaling the spatial coordinates, one can examine the wavefronts at varying degrees of anisotropy, as will be shown below.

A schematic of a planar wavefront incident to a three-dimensional optically-active turbulent-flow region and the irregular wavefront emerging from the flow in three dimensions is shown in figure 10. The distorted wavefront is highly irregular and highly anisotropic. Taking x and y as the spatial directions perpendicular to the incident-wavefront propagation direction, the OPL is in this case a function of x and y as well as time, i.e.

$$\Lambda(x, y, t)\,, \tag{21}$$

where, for simplicity of notation in what follows below, x and y are the spatial coordinates normalized by the large-scale transverse extent L_δ of the flow (cf. figure 10) and Λ is the OPL normalized by $(\Delta n)_{\text{ref}}\, L_\delta$ with $(\Delta_n)_{\text{ref}}$ denoting the reference (freestream) refractive-index difference. To be able to vary the anisotropy of the OPL, which will be needed below, we propose the use of scaling factors (stretching factors) for both the OPL and the spatial coordinates, i.e.

$$\alpha_\Lambda\, \Lambda(\alpha_x\, x\,, \alpha_y\, y\,, t)\,, \tag{22}$$

where α_Λ is a scaling factor for the OPL and $\{\alpha_x, \alpha_y\}$ are scaling factors for the spatial coordinates normal to the incident-wavefront propagation direction. These scaling factors can each be greater than or less than unity. Two examples are shown in figure 11

where different values of α_Λ are employed for the same wavefront or OPL isosurface. We note, with regard to equation 22, that only two wavefront-anisotropy parameters are needed (only the ratios matter) and, therefore, we define a (vector) wavefront-anisotropy parameter given by

$$\boldsymbol{\alpha} \equiv \left\{ \frac{\alpha_\Lambda}{\alpha_x}, \frac{\alpha_\Lambda}{\alpha_y} \right\}, \tag{23}$$

in terms of the ratios of the OPL scaling factor to each of the spatial-coordinate scaling factors. For a wavefront in 2-D space, e.g. in figures 3a and b, only one scaling factor is needed, e.g. $\alpha \equiv \alpha_\Lambda / \alpha_x$.

The proposed wavefront-anisotropy parameter $\boldsymbol{\alpha}$ enables the variation of the effective anisotropy of aerooptical wavefronts which can be used to examine their structure as a function of scale as will be shown below. We note that the above parameter can be used in the study of the isosurfaces of the OPL function as well as in the study of the OPL field itself. In general, the OPL isosurfaces will be different from the OPL field itself. However, for wavefronts emerging from the turbulent shear-flow region, and propagating in an ambient/freestream fluid of uniform refractive index, the wavefronts propagate at constant speed and, to the extent that bending of individual light rays can be ignored, i.e. in the weak aerooptical regime, the optical wavefronts are equivalent to the OPL-field profiles.

To investigate the physical structure of optical wavefronts, a useful approach is to conduct box counting which enables an examination of the manner in which the wavefronts' geometrical features vary with scale ([38] Catrakis *et al.* 2001; [11] Catrakis & Aguirre 2002). For each wavefront, a bounding box or rectangle is identified and partitioned successively into smaller boxes. The number of boxes containing the wavefront is counted at each box scale λ. This coverage count, denoted as $N_d(\lambda)$ in d dimensions, can be used to quantify the geometric structure as a function of scale. At the largest scale $\lambda_{\max}$, the coverage count is unity, i.e. $N_d(\lambda_{\max}) = 1$. We sometimes also denote the largest scale as δ, i.e. the bounding-box scale. One can normalize the coverage count by the total number of boxes available at each scale λ and this is known as the coverage fraction,

$$F_d(\lambda) = \left(\frac{\lambda}{\lambda_{\max}} \right)^d N_d(\lambda), \tag{24}$$

where $0 \leq F_d(\lambda) \leq 1$ and the limiting values correspond to the smallest and largest scales, respectively. The physical meaning of the coverage fraction is that it is the geometric probability of finding a part of the wavefront in a λ-scale box. A larger value of $F_d(\lambda)$, at a given scale, indicates a more irregular wavefront structure at that scale.

Highly-anisotropic behavior can be expected for aerooptical wavefronts, as argued above, and, because of this, the scale λ must be treated as a vector in general, as was proposed for turbulent fluid interfaces in general by Catrakis (2000 [39]), i.e.

$$\boldsymbol{\lambda} = \{\lambda_\Lambda, \lambda_x, \lambda_y\}, \tag{25}$$

with the box scale λ in the general case denoting the magnitude of $\boldsymbol{\lambda}$ which we take as

$$\lambda = (\lambda_\Lambda \lambda_x \lambda_y)^{1/3}, \tag{26}$$

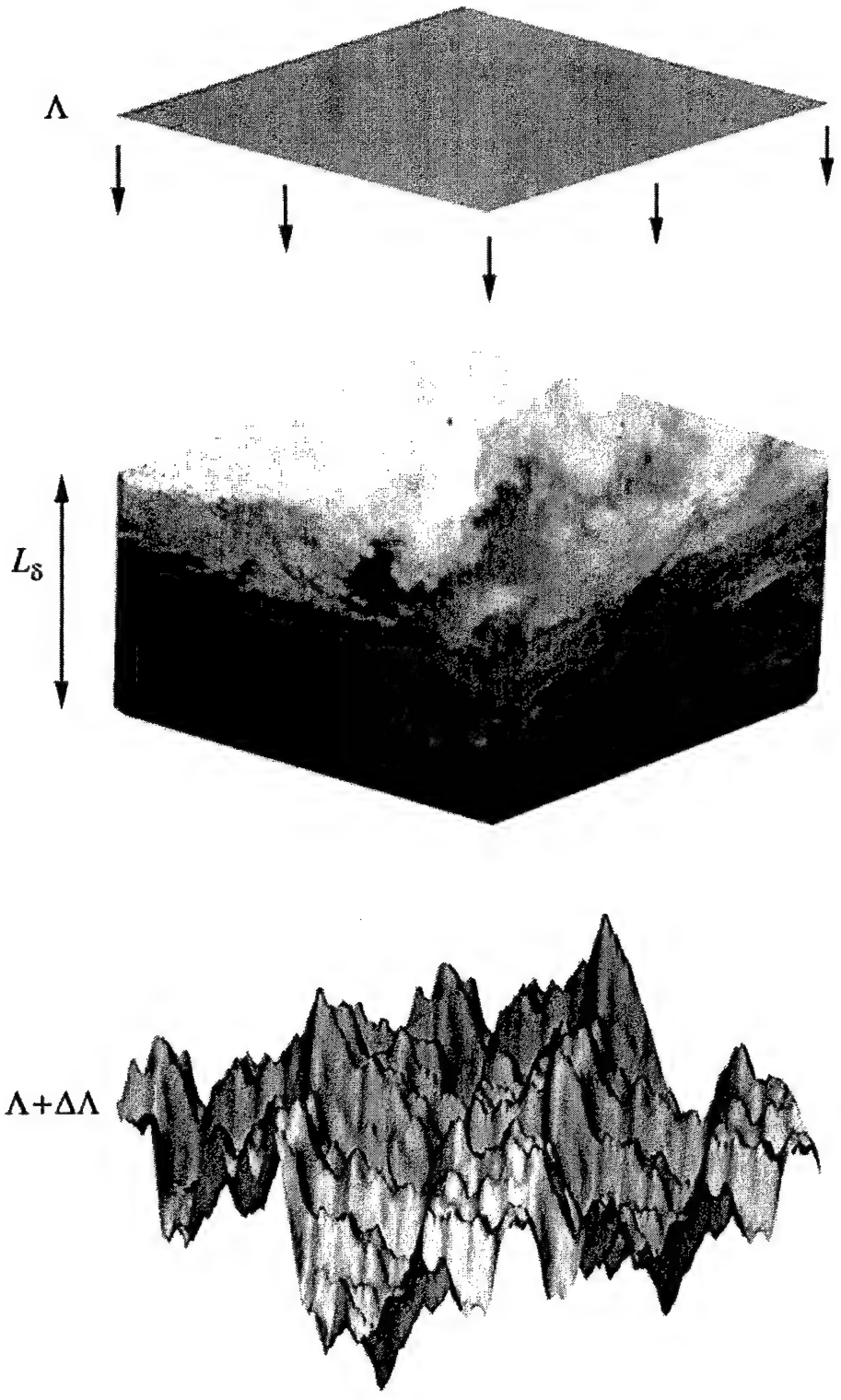

Figure 10: Schematic of a planar optical wavefront (top) incident to a three-dimensional refractive-index field in a large-Reynolds-number turbulent compressible flow (middle), and the emerging highly-irregular aerooptical wavefront (bottom).

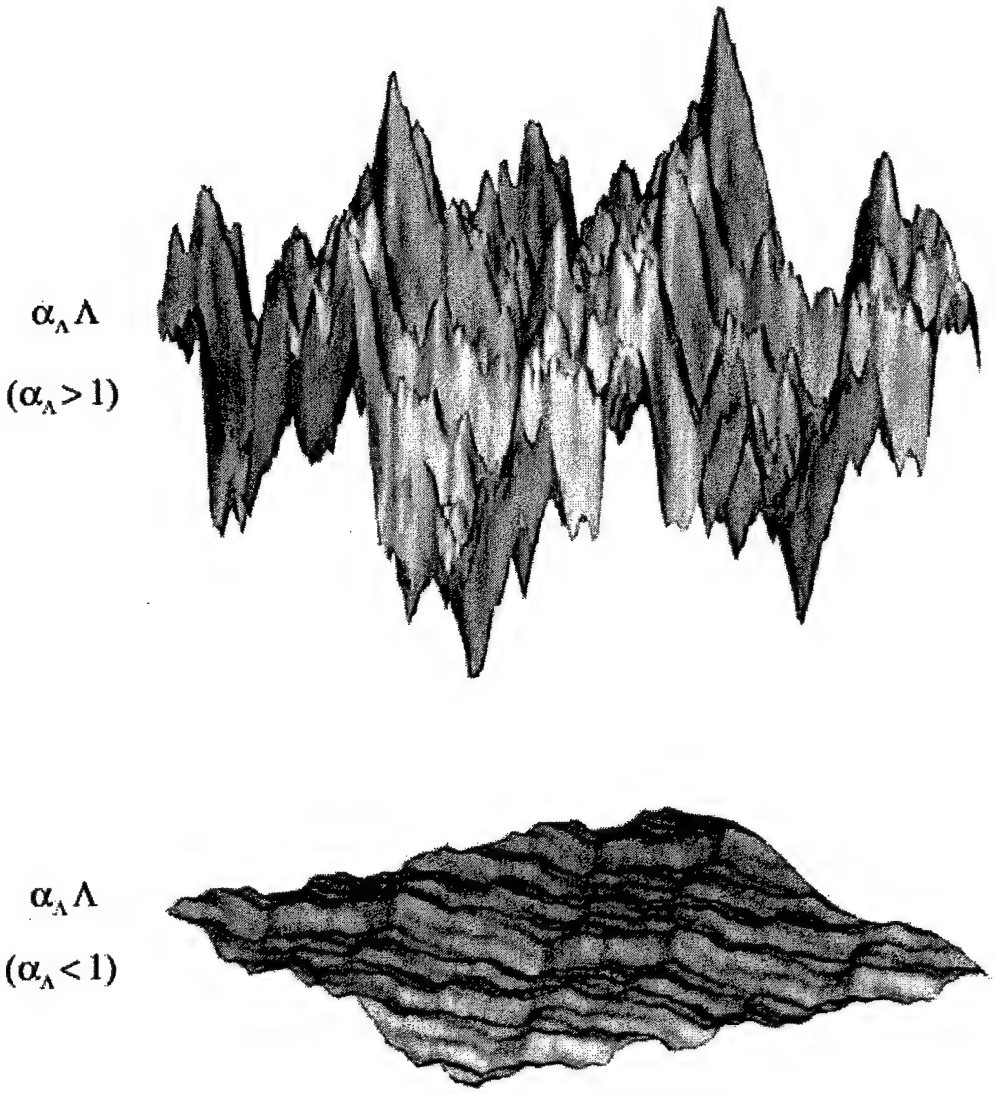

Figure 11: Illustration of varying the effective anisotropy of an optical wavefront in 3-D using the proposed anisotropy parameter $\boldsymbol{\alpha}$, cf. equations 22 and 23. The same wavefront is shown with a relatively-large value of α_Λ (top) and a relatively-small value of α_Λ (bottom).

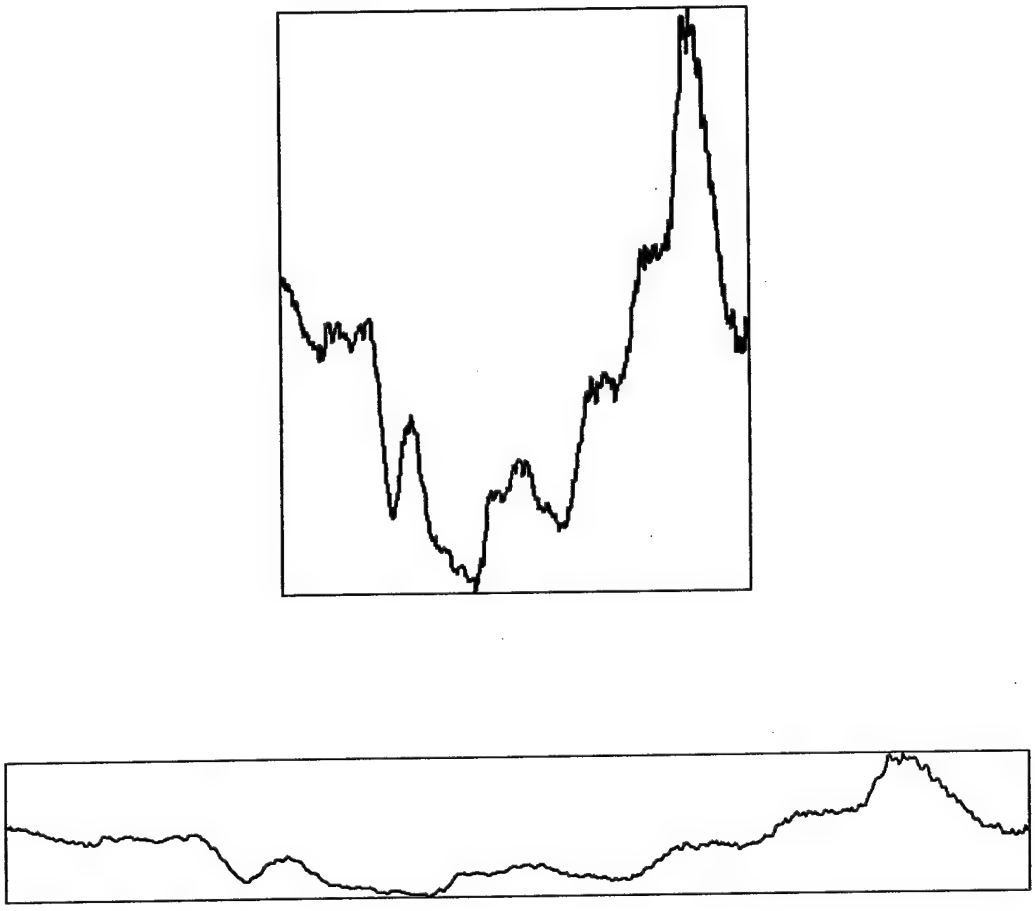

Figure 12: Example of a wavefront in 2-D. The same wavefront is shown at two different values of the anisotropy parameter, which is a scalar-valued parameter in 2-D and is $\alpha = \alpha_\Lambda/\alpha_x$ for this example, such that the large-scale size of the bounding box is the same for each case, i.e. $(\alpha_\Lambda\, \alpha_x)^{1/2}$ is the same.

in 3-D, for example, where λ_Λ denotes the extent of each box in the OPL direction and $\{\lambda_x, \lambda_y\}$ denote the spatial extents of each box in the $\{x, y\}$ directions. The advantage of a scale magnitude defined as in equation 26 is that λ^3 can be identified as a volume occupied by each λ-scale box.

The most important quantity that the box-counting technique produces is the coverage dimension $D_d(\lambda)$ as a function of the scale magnitude λ. The coverage dimension can be computed as the fractional increase in the coverage count per unit fractional decrease in scale, or equivalently the logarithmic derivative of the coverage count with scale, i.e.

$$D_d(\lambda) \equiv -\frac{\mathrm{d}N_d(\lambda)/N_d(\lambda)}{\mathrm{d}\lambda/\lambda} = -\frac{\mathrm{d}\log N_d(\lambda)}{\mathrm{d}\log\lambda}. \tag{27}$$

and can be interpreted as a fractional (fractal) dimension whose departure from the topological dimension d_t of the wavefronts quantifies how complex the wavefront structure is. The coverage dimension must be in the range

$$d_t \leq D_d(\lambda) \leq d, \tag{28}$$

for optical wavefronts. In particular, at the smallest scales and largest scales respectively the coverage dimension reaches those limits, i.e.

$$D_d(\lambda) \to d_t \quad \text{as} \quad \lambda \to \lambda_{\min}, \qquad \text{and}, \qquad D_d(\lambda) \to d \quad \text{as} \quad \lambda \to \lambda_{\max}. \tag{29}$$

For optical wavefronts in 3-D, as indicated in figure 10, these limiting values become $d_t = 2$ and $d = 3$ respectively. For wavefronts in 2-D, cf. figure 12, these values become $d_t = 1$ and $d = 2$ respectively. It is also helpful to think of the *relative* coverage dimension of the wavefronts, i.e. the coverage dimension relative to the topological dimension, which is given by $D_d(\lambda) - d_t$ in general, or $D_2(\lambda) - 1$ in 2-D for example. This is useful for comparing wavefront structure in different dimensions, e.g. in 3-D vs. 2-D, because the values of the relative coverage dimension must range from 0 to 1 independent of whether the wavefront is in a 3-D or 2-D region of the flow, cf. equation 29. Recalling that at large Reynolds numbers one may expect similarity properties over a wide range of scales (cf. equation 17), another important use of the coverage dimension is that it can reveal such similarity properties, including the presence of self-similarity.

If the coverage dimension $D_d(\lambda)$ is a constant over a wide range of scales, then this would mean that the wavefront physically has scale-independent structure in that range of scales and then the wavefront could be modeled using this self-similarity. Specifically, for self-similar behavior the coverage dimension would be $D_d(\lambda) = D_d = \text{const.}$ and the structure of the wavefront could be extrapolated to higher Reynolds numbers (cf. equation 16) using

$$N_d(\lambda) \sim \left(\frac{\lambda_{\max}}{\lambda}\right)^{D_d}, \tag{30}$$

over a wide range of scales $\lambda_{\min} \ll \lambda \ll \lambda_{\max}$ (equation 17). The value of D_d would reflect the complexity of the wavefront structure that statistically repeats itself over a range of scales.

If, however, the coverage dimension is found to be a continuous function of scale throughout the range of scales, then the coverage count would no longer be a power law but instead would behave as

$$N_d(\lambda) \;=\; \exp\left\{ \int_{\lambda}^{\lambda_{\max}} D_d(\lambda') \, \frac{\mathrm{d}\lambda'}{\lambda'} \right\} , \tag{31}$$

as can be readily seen by inverting equation 10. Such scale-dependent behavior, where for example the coverage dimension could be increasing with increasing scale over a range of scales, would mean that the complexity of the wavefront varies with scale. This would mean that more complicated, scale-dependent models would be needed to extrapolate the small-scale structure of optical wavefronts to larger Reynolds numbers. We note, however, that scale-dependent behavior on the basis of $D_d(\lambda)$ alone may not necessarily imply lack of self-similarity. Recent work has indicated that other scale-local measures may be needed to discern self-similar behavior in those cases where $D_d(\lambda)$ appears to be scale dependent ([29] Catrakis, Aguirre, & Ruiz-Plancarte 2002).

As emphasized above, aerooptical wavefronts can be expected to exhibit a strong anisotropy. A more general box-counting approach therefore is needed, to be useful for aerooptics, where one can examine the box-counting behavior of the wavefronts allowing for the possibility that they may be scale independent, i.e. self-similar, in an anisotropic manner. Self-similar anisotropic behavior is often also called self-affine behavior. Self-affine objects have structure which is scale independent but in a manner that depends on the direction. In other words, self-affine objects are anisotropically scale-independent objects whereas self-similar objects are isotropically scale independent.

We propose an anisotropic extension of the box-counting technique whereby the anisotropy parameter $\boldsymbol{\alpha}$ introduced above becomes a parameter in the coverage count and consequently in the coverage fraction as well as in the coverage dimension, i.e.

$$N_d(\lambda;\boldsymbol{\alpha}) \,, \quad \text{and} \,, \quad F_d(\lambda;\boldsymbol{\alpha}) \,, \qquad \text{with} \,, \qquad D_d(\lambda;\boldsymbol{\alpha}) \;=\; -\frac{\mathrm{d}\log N_d(\lambda;\boldsymbol{\alpha})}{\mathrm{d}\log\lambda} \,. \tag{32}$$

The introduction of the anisotropy parameter $\boldsymbol{\alpha}$ in the coverage quantities makes possible a practical examination of anisotropic structure. We note that an equivalent way to proceed would be to treat the scale λ as a vector $\boldsymbol{\lambda}$ (cf. equation 25) and then to define the coverage dimension through an extension of equation 27. This, however, would lead to coverage-dimension vectors expressed as partial derivatives of the coverage count. The proposed approach, i.e. using the quantities in equation 32, offers instead a much simpler way to characterize the anisotropic structure of aerooptical wavefronts, with a coverage dimension that is scalar valued rather than vector valued.

As an example in 2-D, figures 13a and b show the same optical wavefront at two different values of the anisotropy parameter $\boldsymbol{\alpha}$ with the boxes necessary to cover the wavefront in each case for several different scales. The corresponding coverage results are shown in figures 14a, b, and c. Note that the choice of the values of the anisotropy parameter, in figures 13a and b, is such that they both have the same scale magnitudes, i.e. the value of $(\alpha_\Lambda \, \alpha_x)^{1/2}$ is the same for both examples. This was done so that any effects of the largest scales are removed in order to focus on the small-scale structures. Significantly, we see

that for the *same* optical wavefront examined under *different* levels of anisotropy, different behavior is evident at the small scales in figure 14c. This is an important observation because it illustrates that this technique is sensitive to the presence of anisotropy at small scales and, therefore, one can expect to be able to use it to examine aerooptical wavefronts at large Reynolds numbers as will be done below. It is also important to appreciate that the above ideas can be expected to be useful to examine not only the ensemble-averaged structure of the wavefronts but also the *instantaneous* structure of the wavefronts. The latter is particularly important in practical aerooptics applications.

We have demonstrated the use of the proposed anisotropic box-counting technique for the characterization of the small-scale structure of aerooptical distortions. We are particularly interested in the behavior at large Reynolds numbers and high compressibility because this is a flow regime of practical interest in a number of aerooptics applications in high-speed flight, and also because previous work suggests that high-compressibility turbulent flows exhibit important differences at least at the large scales when compared to incompressible or weakly-compressible turbulent flows (e.g. [23] Samimy & Elliot 1990; [18] Papamoschou 1991). Less is known about the effect of compressibility on the small-scale behavior at large Reynolds numbers. Computational results are available on compressible turbulent flows (e.g. [40] Porter, Woodward, & Pouquet 1998) but are presently restricted to low Reynolds numbers. On the theoretical side, there are proposals of similarity and self-similarity properties at large Reynolds numbers (e.g. Sreenivasan 1991) that have been put forth for incompressible turbulence. However, it is presently not clear to what extent such incompressible-turbulence properties are applicable at higher compressibilities.

To examine the applicability of the technique proposed above, we employed recent wavefront data derived from experimental studies of aerooptical distortions in high-compressibility shear layers between different gases ([7] Dimotakis, Catrakis, & Fourguette 2001). In those studies, a large-scale Reynolds number of $Re \sim 10^6$ and a convective Mach number of $M_c \sim 1$ were achieved and the OPL profiles corresponding to wavefronts emerging normal to the shear layers were derived by Fourier filtering the refractive-index field. Two examples of the OPL profiles at these flow conditions are shown in figures 15a and b. The optical-wavefront distortions correspond to the aerooptical interactions in a two-dimensional plane transverse to the shear layer. At the large Reynolds number of these shear layers, there is a wide range of scales (cf. equation 16). Although the wavefront data in figures 6a and b are not fully resolved, the resolution is sufficient to capture a large fraction of the full range of scales. This fraction of the range of scales is estimated to be $\sim 500 : 1$ based on the camera pixel resolution which was employed to record the flow images from which the OPL profiles were derived. Keeping in mind that similarity properties are not expected throughout the entire range of scales smaller than the large scale, but rather in a fraction of those scales (cf. equation 3), these data can be expected to be useful to examine the presence of similarity or self-similarity in the wavefront structure.

For the shear-layer data, the OPL profiles are functions of the streamwise coordinate x

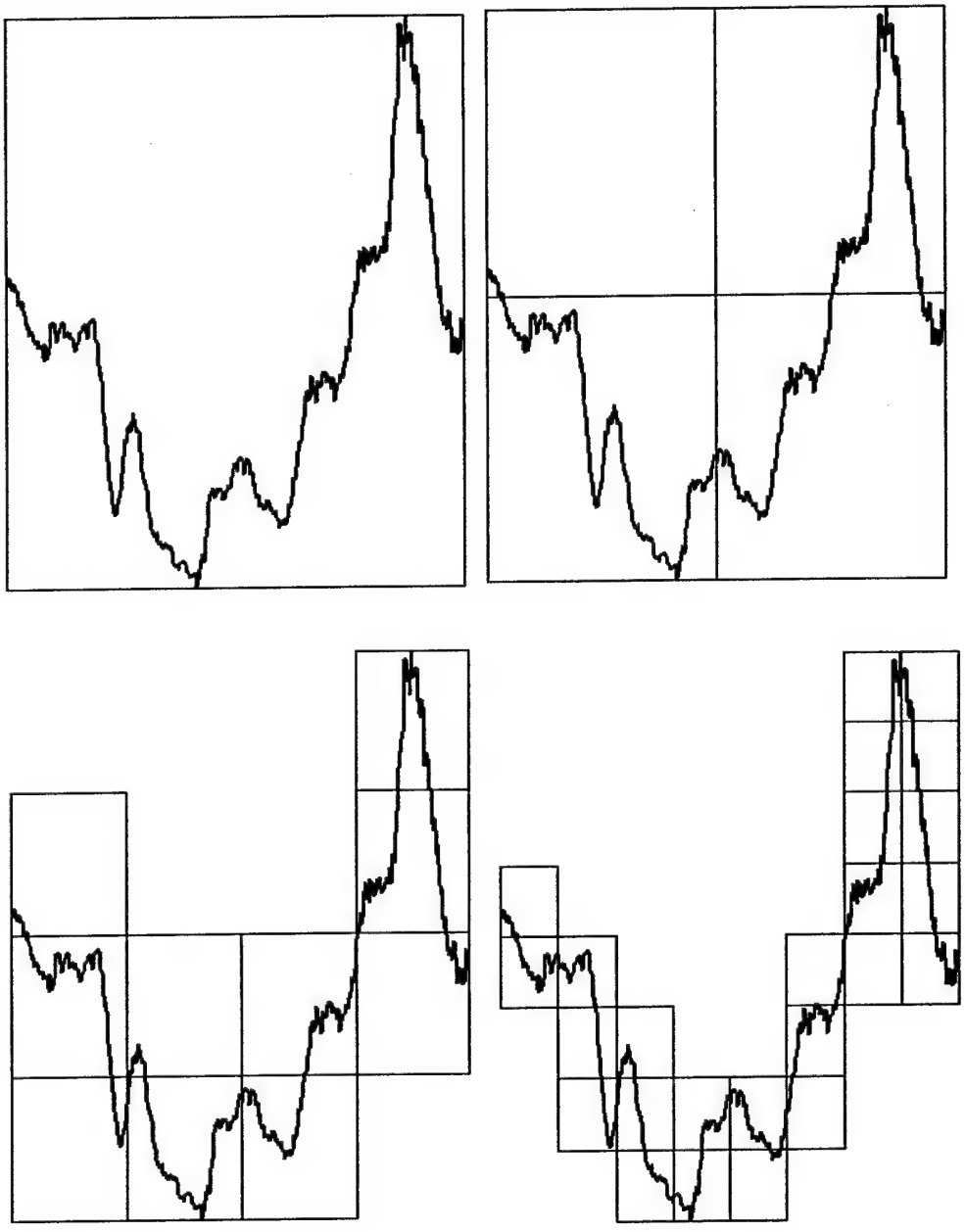

Figure 13: Illustration of the box-counting technique for the wavefront example in figure 12a. Coverage boxes are shown at different scales. The coverage boxes are the boxes needed to completely contain the wavefront at each scale.

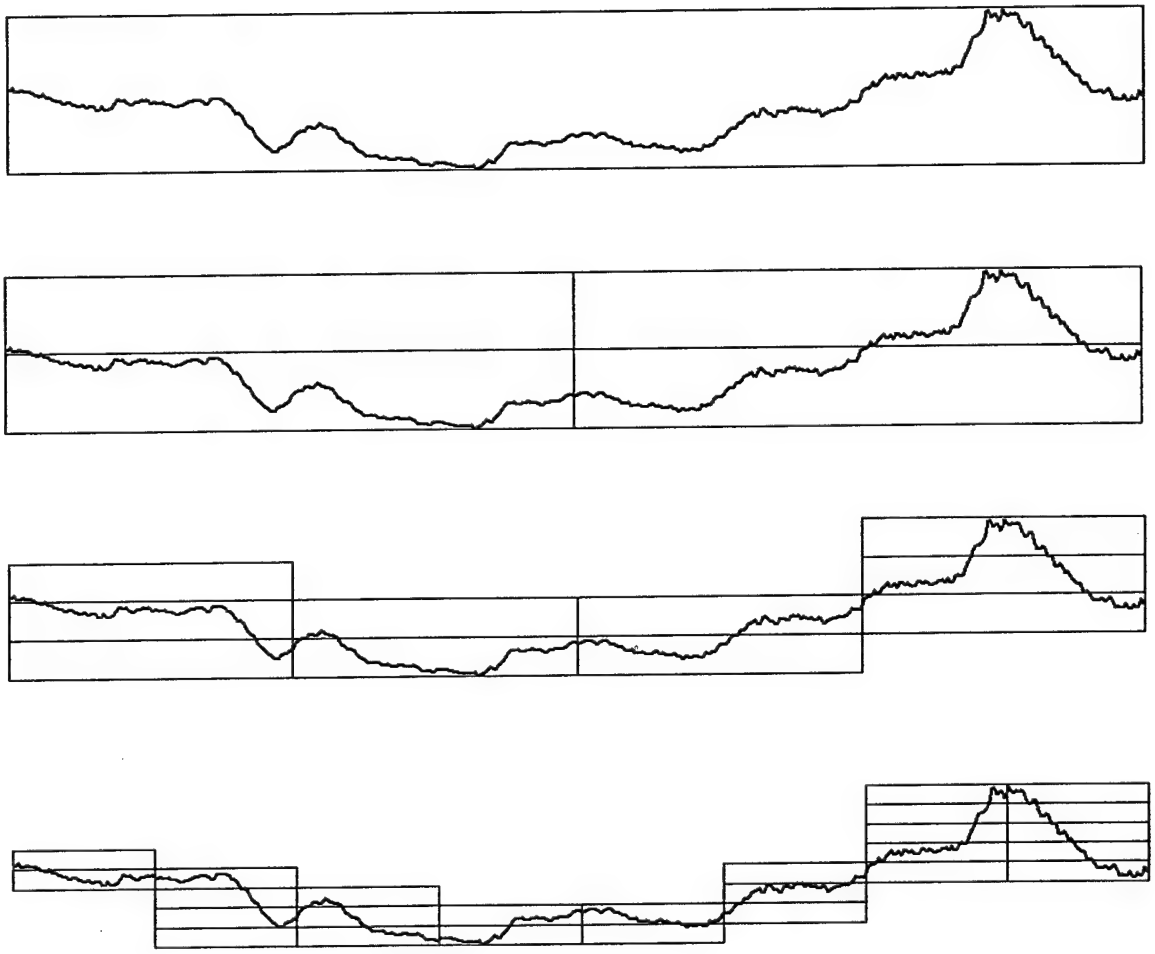

Figure 14: Illustration of the box-counting technique for the wavefront example in figure 12b.

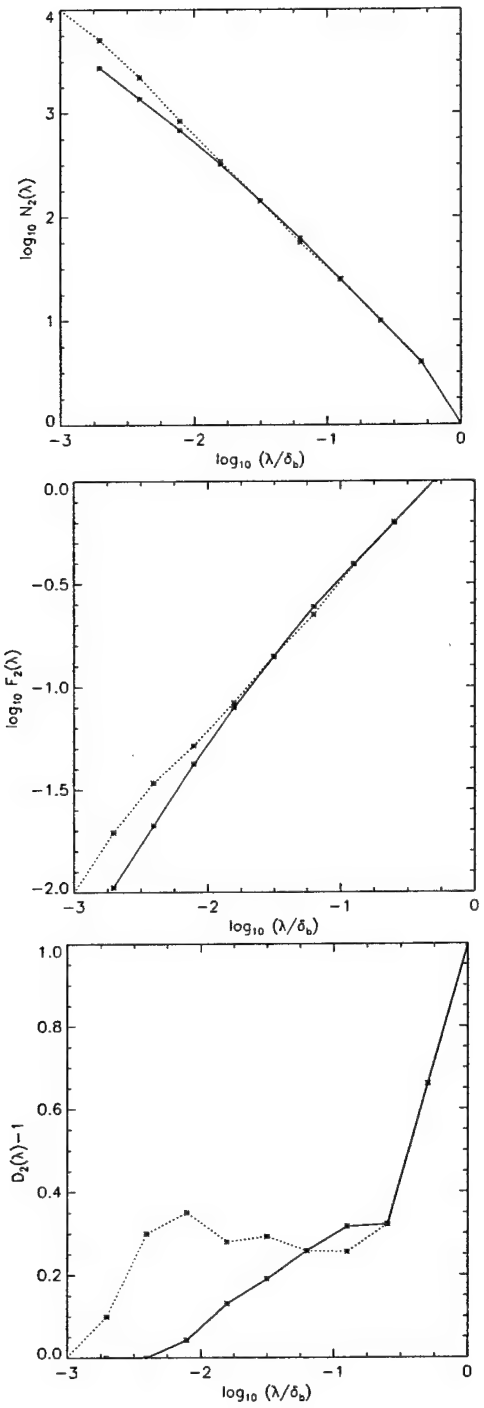

Figure 15: Coverage count (left), coverage fraction (middle), and coverage dimension (right) for the wavefront example in figures 12a and b. The dashed curves correspond to figure 12a, and the solid curves correspond to figure 12b.

normalized by the transverse extent L of the large-scale shear in this flow, i.e.

$$\Lambda\left(\frac{x}{L}\right). \tag{33}$$

The incident wavefronts are assumed to be planar (linear in the plane of the flow studied) so that the coverage dimension is

$$D_2(\lambda) \;=\; 1\,, \tag{34}$$

prior to propagation of the wavefronts through the shear layer. For the propagated and distorted wavefronts, the relevant anisotropic wavefront parameter in this case is

$$\alpha \;\equiv\; \frac{\alpha_\Lambda}{\alpha_x}\,, \tag{35}$$

(cf. equations 22-23), corresponding to the two-parameter stretched-wavefront profile given by

$$\alpha_\Lambda\,\Lambda\left(\alpha_x\,\frac{x}{L}\right). \tag{36}$$

As pointed out above, the two parameters α_Λ and α_x are equivalent to the single parameter $\alpha = \alpha_\Lambda/\alpha_x$. One parameter is sufficient, for wavefronts in 2-D space, to permit an examination of the wavefront structure at different levels of anisotropy.

Box counting was performed on the high-compressibility shear-layer wavefront profiles for several different values of the anisotropy parameter α, over the range $0.3 \lesssim \alpha \lesssim 3$. For each value of α, the wavefront was stretched and subsequently partitioned into boxes (tiles in 2-D) so that the box count was computed as a function of scale, i.e.

$$N_2(\lambda;\alpha)\,, \tag{37}$$

where the subscript 2 denotes that these data are in spatially in two dimensions. From the coverage count, we computed the coverage fraction and the coverage dimension as a function of scale, i.e.

$$F_2(\lambda;\alpha) \;=\; \left(\frac{\lambda}{\lambda_{\max}}\right)^2 N_2(\lambda;\alpha)\,, \quad \text{and}\,, \quad D_2(\lambda;\boldsymbol{\alpha}) \;=\; -\,\frac{\mathrm{d}\log N_2(\lambda;\boldsymbol{\alpha})}{\mathrm{d}\log\lambda}\,. \tag{38}$$

Two important observations were made:

(a) *the small-scale wavefront behavior depends strongly on the anisotropy parameter* α, and

(b) *there exists a particular value of the anisotropy parameter* $\alpha = \alpha^*$ *for which the small-scale wavefront structure is found to be scale independent over a range of scales.*

The first observation confirms the idea above that aerooptical wavefronts are highly anisotropic and shows that the technique described above is capable of detecting the

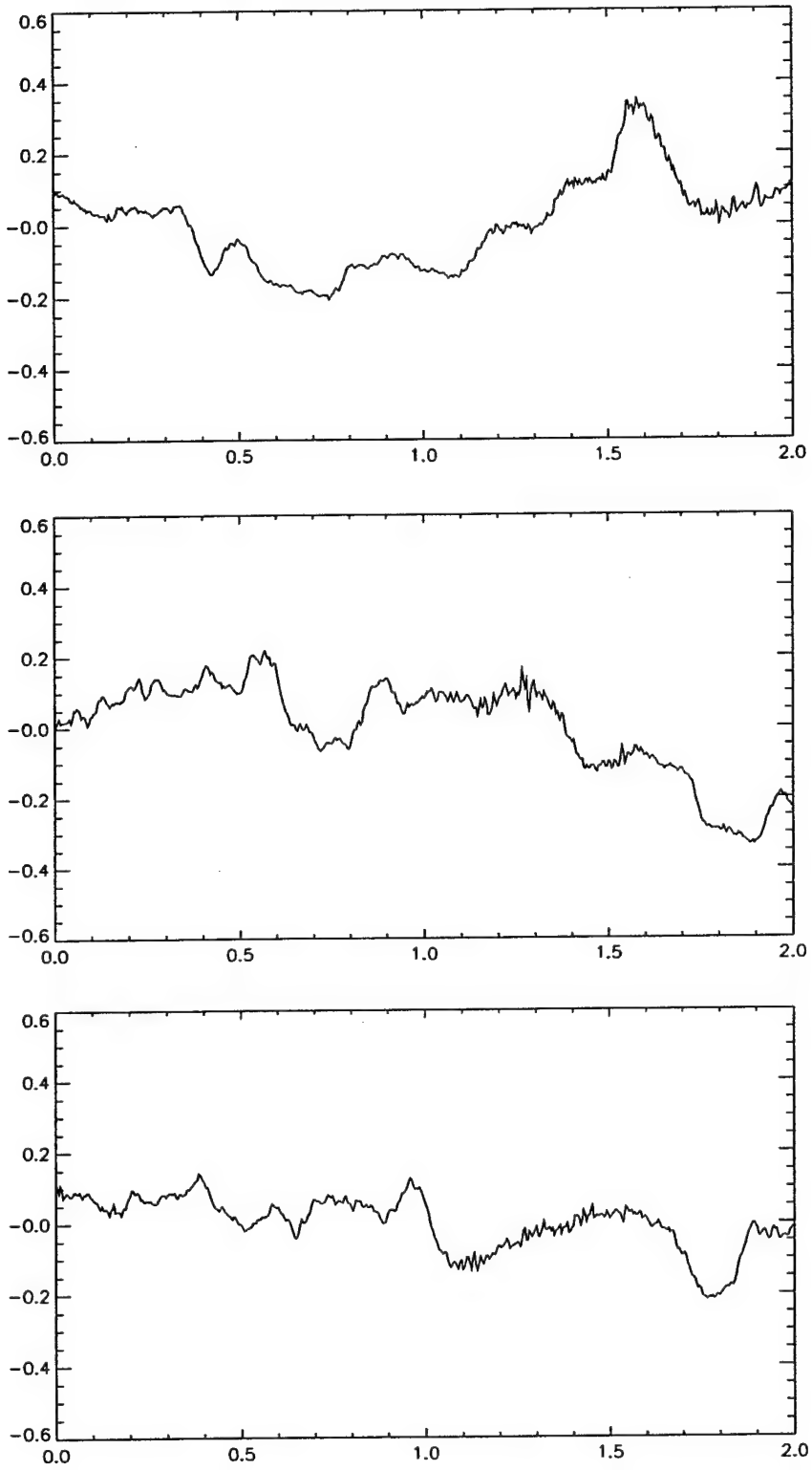

Figure 16: Examples of measurements of optical-wavefront profiles, $\Lambda(x)$, in large-Reynolds-number ($Re \sim 10^6$) high-compressibility ($M_c \sim 1$) shear layers, derived from two-dimensional flow-imaging experiments described in [7]. The wavefront profiles correspond to aerooptical interactions in two-dimensional spatial streamwise slices of the flow.

dependence of the small-scale structure on this anisotropy. The second observation, i.e. that there is scale independence over a range of scales for a particular value α^*, which is found to be $\alpha^* \simeq 0.9$ for the present data, is particularly important. The results are shown in figures 16a, b, and c, that depict respectively the coverage count $N_2(\lambda;\alpha^*)$, coverage fraction $F_2(\lambda;\alpha^*)$, and the relative coverage dimension $D_2(\lambda;\alpha^*) - 1$ for the critical value of the anisotropy parameter. For values of α smaller than or greater than α^*, qualitatively-different behavior was observed. Specifically,

(a) *for $\alpha < \alpha^*$, the wavefront structure is scale dependent with relatively-smaller values of the coverage dimension at intermediate scales,*

(b) *there exists a particular value of the anisotropy parameter $\alpha = \alpha^*$ for which the small-scale wavefront structure is found to be scale independent over a range of intermediate scales.*

(c) *for $\alpha > \alpha^*$, the wavefront structure is scale dependent with relatively-larger values of the coverage dimension at intermediate scales.*

The significance of the observed behavior at $\alpha = \alpha^*$ is that this shows the presence of an intermediate range of scales

$$\lambda_{\text{min}} \ll \lambda \ll \lambda_{\text{max}}\,, \tag{39}$$

in which the wavefront is self-similar, i.e.

$$D_2(\lambda;\alpha^*) \simeq \text{const.} \simeq 1.3\,, \tag{40}$$

in a range of small scales. This can be used to extrapolate the behavior to even higher Reynolds numbers at high compressibility, at least in shear layers, using

$$N_2(\lambda;\alpha^*) \sim \left(\frac{\lambda_{\text{max}}}{\lambda}\right)^{1.3}\,, \tag{41}$$

(cf. equation 16). The uncertainty in the coverage dimension is estimated to be ± 0.025. From figure 16c, we see that the self-similar behavior is evident in the measurements over a range of scales that span approximately one decade. Even though the Reynolds number associated with the shear layer is large, i.e. $Re \sim 10^6$, and corresponds to a full range of flow scales given by $\lambda_{\text{max}}/\lambda_{\text{min}} = Re^{3/4} \sim 3 \times 10^4$, the range of scales over which similarity is expected is smaller. A conservative estimate, for example ([30] Dimotakis 2000), is the ratio of the Taylor scale λ_{T} to the Kolmogorov scale λ_{K} which grows slowly with Reynolds number, specifically $\lambda_{\text{T}}/\lambda_{\text{K}} \sim Re^{1/4} \sim 10$. This estimate, at least of the extent of the range of self-similar scales, is closer to the presently-observed behavior (cf. figure 7c). Higher-resolution measurements would be needed to discern this issue further, i.e. whether the range of scales exhibiting self-similar behavior extends to smaller scales yet. We note that the critical value α^* of the anisotropy parameter might depend to some extent on the Reynolds number and/or Mach number, and possibly on the flow boundary conditions. However, as long as the Reynolds number is large, i.e. meets the criterion for fully-developed turbulence, one can expect that the small-scale structure

of the wavefronts and the critical value of the anisotropy parameter will be at most weakly dependent on these flow parameters. This is because the small-scale structure at large Reynolds numbers is at most weakly sensitive to the large-scale behavior (e.g. [12] Sreenivasan 1991, and references therein).

The present finding of scale independence of the small-scale optical-wavefront structure over a range of scales at high compressibility provides experimental evidence that self-similarity is present in aerooptical interactions at high-compressibility flow conditions. Computational studies of compressible flows at low Reynolds numbers have indicated inertial-range scaling based on power spectra (e.g. [40] Porter, Woodward, & Pouquet 1998) and this supports the present finding of self-similarity, although spectral behavior alone cannot be related uniquely to the physical structure of the fluid interfaces. The present finding of self-similar behavior in the physical structure of the distorted aerooptical wavefronts indicates that turbulent fluid interfaces at high compressibility possess self-similarity properties. Self-similar behavior of the fluid interfaces would be sufficient to explain the observed self-similar aerooptical behavior, with anisotropy inherent in the wavefront OPL.

Quantification and modeling of the physical structure of optical wavefronts, in real space as opposed to Fourier space, requires tools such as the technique presently demonstrated. For wavefronts propagating through spatially three-dimensional regions of turbulent flows, one can expect that the coverage dimension in that case will be

$$D_3 = D_2 + 1, \tag{42}$$

as long as there is self-similarity in a range of scales, in analogy with similar suggestions for turbulent interfaces ([12] Sreenivasan 1991) under the assumption of interfacial self-similarity. In the high-compressibility shear layer, therefore, one can expect that

$$D_3 \simeq 2.3, \tag{43}$$

cf. equation 40. We also note that the values $D_2 \simeq 1.3$ and $D_3 \simeq 2.3$ can be expected to be the same at even larger Reynolds numbers. This is because these values are expected to be Reynolds-number independent as long as the flow is fully developed, which it is in the present case. The present results demonstrate that optical-wavefront self-similarity can be detected using the proposed approach. Two important practical consequences are that one can now extrapolate the physical wavefront structure to even higher Reynolds numbers, using equation 41 throughout the wider range of self-similar scales associated with higher Reynolds numbers, and that the wavefront coverage dimension values of $D_2 \simeq 1.3$ and $D_3 \simeq 2.3$ presently detected at a Reynolds number of $Re \sim 10^6$ can be expected to be valid at higher Reynolds numbers yet.

The proposed method of anisotropic box counting provides a means useful for the characterization of the physical structure of aerooptical wavefronts as a function of scale. The optical-wavefront anisotropy parameter, defined as a ratio of scaling factors for the optical path length (OPL) and spatial extent of the wavefronts, combined with an anisotropic generalization of box counting enables a scale-local examination of wavefronts at varying degrees of anisotropy. This is particularly useful for the study of aerooptical wavefronts at large Reynolds numbers where the distortions span a wide range of

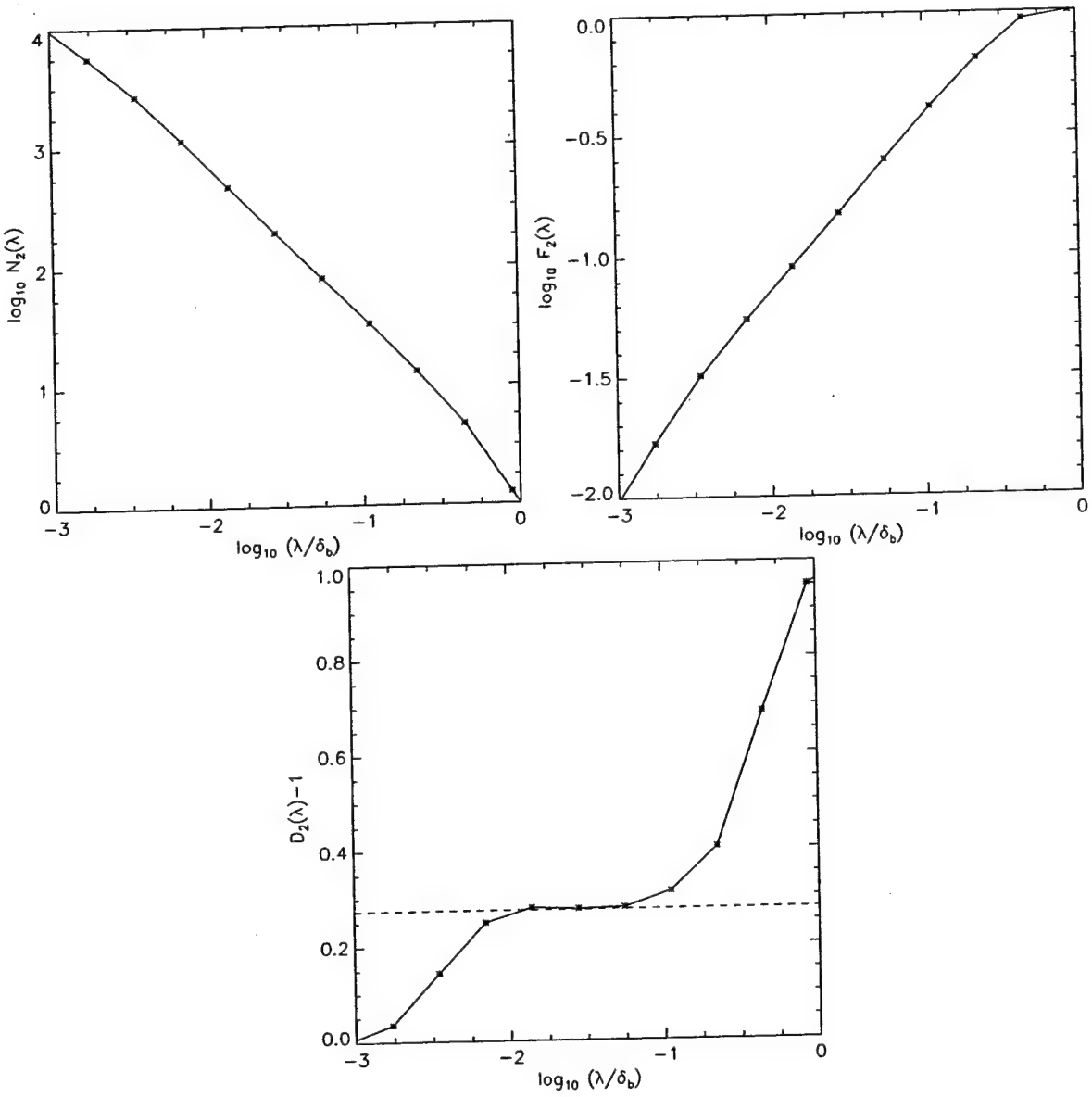

Figure 17: Ensemble-averaged results for optical-wavefront profiles in large-Reynolds-number ($Re \sim 10^6$) high-compressibility ($M_c \sim 1$) shear layers, cf. figures 6a, b, and c: (a) (left) coverage function $N_2(\lambda;\alpha^*)$, (b) (middle) coverage fraction $F_2(\lambda;\alpha^*)$, and (c) (right) relative coverage dimension $D_2(\lambda;\alpha^*)$-1. The value of α^* for the results shown is $\alpha^* \sim 0.9$. The plateau in (c) shows clearly the presence of self-similarity of the wavefront structure over a range of scales spanning approximately one decade.

scales and are anisotropic. Demonstration of this technique to experimental data in large-Reynolds-number ($Re \sim 10^6$) high-compressibility ($M_c \sim 1$) turbulent shear layers shows the presence of anisotropic self-similarity in the wavefront structure over a range of small scales. This finding is particularly important because it provides a means to extrapolate the small-scale structure of aerooptical distortions at high compressibility to larger Reynolds numbers. This can be expected to be particularly useful in efforts to develop computational models and simulations of aerooptical interactions at large Reynolds numbers and high compressibility (e.g. [26] Jones & Bender 2001), because the present self-similarity model of the wavefront distortions provides a key ingredient to construct effective sub-grid-scale aerooptics models in large-eddy aerooptics simulations. Such aerooptical properties for high-compressibility flows can be expected to be especially valuable in applications involving high-resolution and/or long-range optical imaging and beam propagation at high-speed flight.

References

[1] H. J. Catrakis and R. C. Aguirre. New interfacial-thickness approach in aerooptics and large-scale optical distortions in high-compressibility turbulence. *AIAA J.*, 2003. Submitted for publication.

[2] H. J. Catrakis, R. C. Aguirre, and J. Ruiz-Plancarte. Aerooptical-wavefront anisotropy and small-scale structure at large Reynolds numbers and high compressibility. *AIAA J.*, 2003. Submitted for publication.

[3] E. J. Jumper and E. J. Fitzgerald. Recent advances in aerooptics. *Prog. Aerospace Sci.*, 37:299–339, 2001.

[4] K. G. Gilbert and L. J. Otten. Aero-optical phenomena. In *Progress in Astronautics and Aeronautics*, volume 80. American Institute of Aeronautics and Astronautics, 1982.

[5] C. R. Truman and M. J. Lee. Effects of organized turbulence structures on the phase distortion in a coherent optical beam propagating through a turbulent shear flow. *Phys. Fluids A*, 2:851–857, 1990.

[6] J. B. Wissler and A. Roshko. Transmission of thin light beams through turbulent mixing layers. In *AIAA 30th Aerospace Sciences Meeting, AIAA-92-0658*, Reno, NV, 1992.

[7] P. E. Dimotakis, H. J. Catrakis, and D. C. L. Fourguette. Flow structure and optical beam propagation in high-Reynolds-number gas-phase shear layers and jets. *J. Fluid Mech.*, 433:105–134, 2001.

[8] A. J. Smits and J.-P. Dussauge. *Turbulent Shear Layers in Supersonic Flow.* AIP Press, 1996.

[9] H. W. Liepmann. Aspects of the turbulence problem. Part 2: IV. General discussion, V. Isotropic turbulence,. *Z. angew. Math. Phys.*, 3:407–426, 1952.

[10] H. W. Liepmann. Deflection and diffusion of a light ray passing through a boundary layer. Douglas Aircraft Company Report SM-14397, Santa Monica, CA, 1952.

[11] H. J. Catrakis and R. C. Aguirre. Inner-scale structure of turbulence-degraded optical wavefronts. In *AIAA 33rd Plasmadynamics and Lasers Conference, AIAA 2002-2269*, Maui, HI, 2002.

[12] K. R. Sreenivasan. Fractals and multifractals in fluid turbulence. *Annu. Rev. Fluid. Mech.*, 23:539–600, 1991.

[13] E. J. Jumper and R. J. Hugo. Quantification of aero-optical phase distortion using the small-aperture beam technique. *AIAA J.*, 33:2151–2157, 1995.

[14] E. J. Fitzgerald and E. J. Jumper. Scaling aero-optic aberrations due to propagation through compressible shear layers. In *AIAA 2000-2354*, 2000.

[15] G. L. Brown and A. Roshko. On density effects and large scale structure in turbulent mixing layers. *J. Fluid Mech.*, 64:775–816, 1974.

[16] L. Chew and W. Christiansen. Coherent structure effects on optical performance of plane shear layers. *AIAA J.*, 29:76–80, 1991.

[17] D. Papamoschou and Roshko A. The compressible turbulent shear layer: an experimental study. *J. Fluid Mech.*, 197:453–477, 1988.

[18] D. Papamoschou. Structure of the compressible turbulent shear layer. *AIAA J.*, 29:680–681, 1991.

[19] N. T. Clemens and M. G. Mungal. Large-scale structure and entrainment in the supersonic mixing layer. *J. Fluid Mech.*, 284:171–216, 1995.

[20] R. C. Aguirre, J. Ruiz-Plancarte, and H. J. Catrakis. Physical thickness of turbulent fluid interfaces: structure, variability, and applications to aerooptics. In *AIAA 41st Aerospace Sciences Meeting and Exhibit, AIAA 2003-0642*, Reno, Nevada, 2003.

[21] R. Samtaney, D. I. Pullin, and B. Kosović. Direct numerical simulation of decaying compressible turbulence and shocklet statistics. *Phys. Fluids*, 13:1415–1430, 2001.

[22] D. Bogdanoff. Compressibility effects in turbulent shear layers. *AIAA J.*, 21:926–927, 1983.

[23] M. Samimy and G. S. Elliot. Effects of compressibility on the characteristics of free shear layers. *AIAA J.*, 28:439–445, 1990.

[24] M. Samimy, M. F. Reeder, and G. S. Elliot. Compressibility effects on large structures in free shear flows. *Phys. Fluids*, 4:1251–1258, 1992.

[25] B. Thurow, M. Samimy, W. Lempert, S. R. Harris, J. Widiker, and B. Duncan. Simultaneous MHz rate flow visualization and wavefront sensing for aerooptics. In *AIAA 41st Aerospace Sciences Meeting & Exhibit, AIAA 2003-0684*, Reno, NV, 2003.

[26] M. Jones and E. E. Bender. CFD-based computer simulation of optical turbulence through aircraft flowfields and wakes. In *AIAA 32rd Plasmadynamics and Lasers Conference, AIAA 2001-2798*, Anaheim, CA, 2002.

[27] M. Stanek, N. Sinha, J. Seiner, B. Pearce, and M. Jones. Applying very high frequency excitation to the problem of tactical directed energy beam propagation. In *AIAA 33rd Plasmadynamics and Lasers Conference, AIAA 2002-2272*, Maui, HI, 2002.

[28] J. P. Siegenthaler, E. J. Jumper, and A. Asghar. A preliminary study in regularizing the coherent structures in a planar, weakly-compressible, free shear layer. In *AIAA 41st Aerospace Sciences Meeting & Exhibit, AIAA 2003-0680*, Reno, NV, 2003.

[29] H. J. Catrakis, R. C. Aguirre, and J. Ruiz-Plancarte. Area–volume properties of fluid interfaces in turbulence: scale-local self-similarity and cumulative scale dependence. *J. Fluid Mech.*, 462:245–254, 2002.

[30] P. E. Dimotakis. The mixing transition in turbulent flows. *J. Fluid Mech.*, 409:69–98, 2000.

[31] H. G. E. Hentschel and I. Procaccia. Passive scalar fluctuations in intermittent turbulence with applications to wave propagation. *Phys. Rev. A.*, 28:417–426, 1983.

[32] C. Schwartz, G. Baum, and E. N. Ribak. Fractal character of turbulence-degraded wavefronts. In *8th Meeting on Optical Engineering and Remote Sensing, SPIE Proceedings, Vol. 1971*, pages 476–485, Tel Aviv, Israel, 1993.

[33] C. Schwartz, G. Baum, and E. N. Ribak. Turbulence-degraded wave fronts as fractal surfaces. *J. Opt. Soc. Am.*, 11(1):444–451, 1994.

[34] A. N. Kolmogorov. The local structure of turbulence in incompressible viscous fluid for very large Reynolds numbers. *Dokl. Akad. Nauka SSSR*, 30:301–305, 1941.

[35] G. I. Taylor. Statistical theory of turbulence. Parts i-iv. *Proc. R. Soc. Lond.* A, 151:421–478, 1935.

[36] L. F Richardson. *Weather Prediction by Numerical Process.* Cambridge University Press, 1922.

[37] L. C. Andrews and R. L. Phillips. *Laser beam propagation through random media.* SPIE Optical Engineering Press, Bellingham, WA, 1998.

[38] H. J. Catrakis, R. C. Aguirre, R. D. Thayne, B. A. McDonald, and J. W. Hearn. Are turbulence-degraded optical wavefronts and beam trajectories fractal? In *AIAA 32nd Plasmadynamics and Lasers Conference, AIAA 2001-2801*, Anaheim, CA, 2001.

[39] H. J. Catrakis. Distribution of scales in turbulence. *Phys. Rev.* E, 62:564–578, 2000.

[40] D. H. Porter, P. R. Woodward, and A. Pouquet. Inertial range structures in decaying compressible turbulent flows. *Phys. Fluids*, 10:237–245, 1998.